Table 2. The result of genome wide association analysis of age at menarche.

SNP	Chr	Position	Gene	allele		Allele 1 freq.	Beta	SE	P
				1	2				
rs364663	6	105549882	*LIN28B*	A	T	0.71679	−0.0893	0.01784	5.49×10^{-7}
rs12200251	6	105489108	*LIN28B*	A	G	0.71854	−0.0868	0.01775	1.00×10^{-6}
rs314263	6	105499438	*LIN28B*	T	C	0.71852	−0.0867	0.01775	1.03×10^{-6}
rs2095812	6	105490671	*LIN28B*	G	C	0.28544	0.08667	0.01777	1.08×10^{-6}
rs7759938	6	105485647	*LIN28B*	T	C	0.71771	−0.0865	0.01777	1.12×10^{-6}
rs4946651	6	105476203	*LIN28B*	A	G	0.27974	0.08708	0.0179	1.15×10^{-6}
rs11156429	6	105471114	*LIN28B*	T	G	0.28116	0.08646	0.01782	1.22×10^{-6}
rs9391253	6	105474309	*LIN28B*	A	T	0.71867	−0.0865	0.01782	1.22×10^{-6}
rs314262	6	105501314	*LIN28B*	A	G	0.71838	−0.086	0.01775	1.26×10^{-6}
rs314280	6	105507530	*LIN28B*	A	G	0.28161	0.086	0.01775	1.26×10^{-6}
rs395962	6	105504111	*LIN28B*	T	G	0.28161	0.086	0.01775	1.26×10^{-6}
rs314274	6	105519625	*LIN28B*	A	C	0.28305	0.08279	0.01709	1.28×10^{-6}
rs1744206	6	105530624	*LIN28B*	G	C	0.28307	0.08271	0.01709	1.31×10^{-6}
rs314266	6	105528010	*LIN28B*	T	C	0.71684	−0.0827	0.01709	1.31×10^{-6}
rs314268	6	105524671	*LIN28B*	A	G	0.71677	−0.0827	0.01709	1.31×10^{-6}
rs314290	6	105533687	*LIN28B*	A	G	0.283	0.08263	0.01709	1.34×10^{-6}
rs314291	6	105531594	*LIN28B*	T	C	0.71699	−0.0826	0.01709	1.34×10^{-6}
rs314289	6	105537627	*LIN28B*	T	C	0.71703	−0.0825	0.01709	1.39×10^{-6}
rs314276	6	105514692	*LIN28B*	A	C	0.28276	0.08522	0.01775	1.57×10^{-6}
rs167539	6	105516741	*LIN28B*	A	C	0.71714	−0.0851	0.01775	1.61×10^{-6}
rs7114000	11	126112790	*KIRREL3*	A	G	0.06837	0.15025	0.03164	2.04×10^{-6}
rs3862645	11	126113656	*KIRREL3*	A	G	0.06837	0.15019	0.03164	2.07×10^{-6}
rs314270	6	105569569	*LIN28B*	T	C	0.2829	0.0843	0.01777	2.10×10^{-6}
rs314272	6	105568697	*LIN28B*	A	G	0.71716	−0.084	0.01777	2.26×10^{-6}
rs314273	6	105568575	*LIN28B*	T	G	0.28266	0.08396	0.01777	2.31×10^{-6}
rs1106419	11	126114297	*KIRREL3*	A	G	0.06846	0.14829	0.0318	3.12×10^{-6}
rs12800752	11	99911850	*ARHGAP42*	T	C	0.80147	0.09455	0.02028	3.12×10^{-6}
rs310008	16	80031150	*CMIP*	G	C	0.13392	−0.1076	0.02322	3.57×10^{-6}
rs6431393	2	236204046	*AGAP1*	A	G	0.4948	0.07757	0.01681	3.95×10^{-6}
rs4735738	8	77774180	*ZFHX4*	A	G	0.49918	0.07283	0.01594	4.93×10^{-6}
rs3862642	11	126110244	*KIRREL3*	T	C	0.06969	0.1438	0.03149	4.97×10^{-6}
rs6995390	8	77773567	*ZFHX4*	A	T	0.49503	0.07271	0.01597	5.30×10^{-6}
rs3889461	11	126113915	*KIRREL3*	T	C	0.93023	−0.1426	0.03149	5.98×10^{-6}
rs9404590	6	105507706	*LIN28B*	T	G	0.77319	−0.0847	0.01879	6.49×10^{-6}
rs7822501	8	77825351	*ZFHX4*	A	G	0.51105	0.06865	0.01529	7.16×10^{-6}
rs7822914	8	77825593	*ZFHX4*	T	C	0.48895	−0.0687	0.01529	7.16×10^{-6}
rs6472982	8	77825957	*ZFHX4*	T	C	0.48894	−0.0685	0.01529	7.44×10^{-6}
rs2076751	14	36059170	*NKX2-1*	A	C	0.23377	−0.087	0.01941	7.45×10^{-6}
rs6472983	8	77834432	*ZFHX4*	T	G	0.48902	−0.0685	0.01529	7.56×10^{-6}
rs369065	6	105550751	*LIN28B*	T	C	0.65066	−0.0721	0.01615	7.92×10^{-6}
rs1865294	8	77772597	*ZFHX4*	A	G	0.50188	0.07121	0.01599	8.41×10^{-6}
rs7114467	11	15414043	*INSC*	A	G	0.45957	−0.0713	0.01601	8.52×10^{-6}

Genotyping result of 15,495 Japanese subjects were anlayzed in this study. Imputed SNPs with R2 of less than 0.7 were excluded from this analysis. A1 frequency of JPT was those from release 24 Hapmap JPT.

*Effect size and SE of allele1 on age at menarche (year per allele) and P-values were obtained by inverse-variance method.

doi:10.1371/journal.pone.0063821.t002

Table 3. Association of rs364663 with age at menarche.

Groups	Chr	allele		Number of samples	Allele 1 Freq.	Beta*	SE*	P
	Position	1	2					
Cohort1		A	T	11454	0.72	−0.069	0.021	7.71×10^{-4}
Cohort2	6			941	0.71	−0.131	0.068	0.056
Cohort3				1957	0.72	−0.137	0.050	0.0064
Cohort4	105549882			1143	0.71	−0.163	0.060	0.0071
Metaanalysis *				15495	0.72	−0.089	0.018	5.49×10^{-7}

*Effect size and S.E. of allele1 on age at menarche (year per allele) and P-values were obtained by inverse-variance method.

doi:10.1371/journal.pone.0063821.t003

Through the analysis of more than 15,000 Japanese female subjects from the Biobank Japan Project, we here report the association of *LIN28B* with AAM. In our analysis, SNP rs364663 within intron 2 of the *LIN28B* gene exhibited the strongest association. Previously reported SNPs rs314263, rs7759938, rs314280, and rs314276 near or in the *LIN28B* gene also showed equivalent association with p-values of $1.03-1.57\times10-6$. Although the directions of associations were consistent between women of European ancestry and those of Japanese, the effect sizes among Japanese (0.085–0.087) were less than those among European ancestry (0.09–0.14). Thus *LIN28B* is a common AAM loci, but its effects are relatively small among the Japanese population.

The lin-28 gene was originally identified through C. elegans mutants showing abnormality in developmental timing [43]. Deleterious mutations in lin-28 produce an abnormal rapid tempo of development through larval stages to adult cuticle formation [43]. Two mammalian homologs, Lin28a and Lin28b, possess similar biochemical activities [44,45]. Transgenic mice expressing Lin28a exhibited increased body size, crown-rump length and delayed onset of puberty due to increased glucose metabolism and insulin sensitivity [46]. In humans, both *LIN28B* and *LIN28A* control preprocessing of the let7 microRNA family [45]. *Lin28B* is highly expressed in the majority of human hepatocellular carcinomas and embryonic stem cells [47], and regulate cell pluripotency [48] as well as cancer growth [47]. However the role of genetic variations in the *LIN28B* locus should be investigated in the future study.

Among the seven suggestive loci indentified in our GWAS, *ZFHX4* and *NKX2.1* loci were previously shown to be associated with height in the Caucasian population [49,50]. These loci also exhibited association with height among the Japanese population ($p = 0.053$ and 0.023, respectively). The *NKX2.1* gene encodes a thyroid-specific transcription factor that was shown to be associated with hypothyroidism [51]. Since delayed pubertal development is a common manifestation of hypothyroidism, variation at *NKX2.1* locus might affect AAM through the regulation of serum thyroid hormone level. The *ZFHX4* gene encodes a homeodomain-zinc finger protein. *ZFHX4* mRNA is highly expressed in brain, liver, and muscle, however the molecular mechanism whereby variations within this genetic locus affect AAM is not clear. In addition, *KIRREL3* locus was shown to be associated with breast size in women of European ancestry [52]. The *KIRREL3* gene encode a member of the nephrin-like protein family. *KIRREL3* was highly expressed in brain and kidney, and shown to be associated with mental retardation autosomal dominant type 4 [53] and neurocognitive delay associated with Jacobsen Syndrome [54]. Taken together, these three loci seem to be common development traits in women of both European ancestry and Japanese.

In our candidate analysis, the association of SNPs rs4452860 and rs7028916 on 9q31.2 with AAM was also validated. This locus was repeatedly shown to be associated with AAM [25,55]as well as serum ALT (alanine transaminase) level[56]. SNPs rs4452860 and rs7028916 were located more than 300 kb away from the *TMEM38B* gene. In mice, *TMEM38B* is strongly expressed in brain, and *TMEM38B* deficient mice is neonatal lethal[57]. In humans, a homozygous mutation of *TMEM38B* was associated with autosomal recessive osteosgenesis imperfecta[58]. These findings also suggest an important role of TMEM38B in developmental processes.

In this study, we observed early AAM among breast cancer patients compared with overall samples (12.99 vs 13.44, **Table S1**). On the other hand, patients with osteoporosis exhibited late AAM (14.33 y.o.). These findings are concordant with previous reports. Since we do not have age-matched controls, the association of these diseases and AAM should be examined using more appropriate sample sets.

Although more than 15,000 samples were employed in this study, no SNP cleared the genome wide significance threshold ($p<5\times10^{-8}$). This could be explained by some limitations in our study. Firstly, the information about AAM was self-reported and might not be very accurate. Although this distinct event is often well recalled many years later [59], possible error due to age-associated memory impairment would increase the risk of false negative association. Secondly, we did not have a replication sample set, and the total sample size may be inadequate to detect variations with modest effects. At present, we unfortunately do not have sufficient samples for replication, since more than 2,900 additional samples are necessary to obtain a genome wide significant association for the top SNP rs364663. Previous studies comprising up to 17,510 women detected only one or two genome-wide significant signals [22–25]. However, 30 significant loci were identified by using 87,802 subjects in the screening stage [21]. Although no SNPs reached the genome wide significance in our study, analyzing an increased number of subjects in a relatively younger generation would improve statistical power as well as data accuracy, and subsequently enable us to identify other genetic factors with modest effects.

Methods

Samples

The subjects enrolled in the GWAS meta-analysis for age at menarche (AAM) ($n = 15,495$) consisted of female patients that were classified into 33 disease groups; cancer (lung, esophagus, stomach, colon, liver, cholangiocarcinoma, pancreas, breast,

Table 4. Association results in Japanese woman of previously identified SNPs with age at menarche in Caucasian woman.

SNP	Chr	Position	Gene	allele		Allele 1 freq.	Beta*	S.E.*	P	ref	concordance**
				1	2						
rs466639	1	163,661,506	*RXRG*	T	C	0.204	−0.0431	0.0196	0.028	1)	yes
rs633715	1	176,119,203	*SEC16B*	T	C	0.779	0.0312	0.0188	0.097	1)	yes
rs2947411	2	604,168	*TMEM18*	A	G	0.096	0.0519	0.0268	0.053	1)	yes
rs17268785	2	56,445,587	*CCDC85A*	A	G	0.793	−0.0561	0.0196	0.004	1)	yes
rs17188434	2	156,805,022	*NR4A2*	N.D.						1)	N.D.
rs12617311	2	199,340,810	*PLCL1*	A	G	0.432	−0.0026	0.0174	0.883	1)	yes
rs7617480	3	49,185,736	*KLHDC8B*	N.D.						1)	N.D.
rs6762477	3	50,068,213	*RBM6*	A	G	0.858	0.0219	0.0250	0.380	1)	yes
rs7642134	3	86,999,572	*VGLL3*	A	G	0.463	−0.0167	0.0173	0.334	1)	yes
rs6438424	3	119,057,512	*LOC100421670*	A	C	0.370	−0.0455	0.0162	0.005	1)	yes
rs6439371	3	134,093,442	*TMEM108, NPHP3*	A	G	0.705	−0.0080	0.0178	0.655	1)	yes
rs2002675	3	187,112,262	*TRA2B, ETV5*	A	G	0.862	−0.0128	0.0231	0.581	1)	yes
rs13187289	5	133,877,076	*PHF15*	G	C	0.078	0.0440	0.0295	0.137	1)	yes
rs13357391	5	136,468,981	*SPOCK*	T	C	0.840	−0.0248	0.0221	0.262	3)	yes
rs1859345	5	136,475,319	*SPOCK*	T	C	0.838	−0.0213	0.0221	0.336	3)	yes
rs4840086	6	100,315,159	*PRDM13, MCHR2*	A	G	0.619	−0.0251	0.0161	0.118	1)	no
rs1361108	6	126,809,293	*C6orf173, TRMT11*	N.D.						1)	N.D.
rs1079866	7	41,436,618	*INHBA*	G	C	0.298	0.0150	0.0170	0.376	1)	yes
rs7821178	8	78,256,392	*PXMP3*	A	C	0.436	−0.0150	0.0170	0.380	1)	yes
rs4452860	9	107,965,210	*TMEM38B*	A	G	0.545	0.0513	0.0160	0.0013	2)	yes
rs7028916	9	107,966,889	*TMEM38B*	A	C	0.454	−0.0512	0.0160	0.0013	2)	yes
rs7861820	9	107,976,495	*TMEM38B*	T	C	0.204	0.0363	0.0196	0.064	2)	yes
rs2090409	9	108,006,909	*TMEM38B*	N.D.						1)	N.D.
rs12684013	9	108,037,935	*TMEM38B*	T	C	0.525	−0.0265	0.0160	0.099	2)	yes
rs10980926	9	113,333,455	*ZNF483*	A	G	0.633	0.0441	0.0161	0.006	1)	yes
rs4929923	11	8,595,776	*TRIM66*	T	C	0.624	0.0068	0.0161	0.674	1)	yes
rs900145	11	13,250,481	*ARNTL*	T	C	0.489	−0.0371	0.0160	0.020	1)	yes
rs10899489	11	77,773,021	*GAB2*	A	C	0.439	0.0257	0.0160	0.109	1)	yes
rs6589964	11	122,375,893	*BSX*	A	C	0.549	−0.0137	0.0183	0.453	1)	yes
rs6575793	14	100,101,970	*BEGAIN*	T	C	0.328	−0.0279	0.0179	0.119	1)	yes
rs1659127	16	14,295,806	*MKL2*	A	G	0.483	0.0085	0.0161	0.595	1)	yes
rs9939609	16	52,378,028	*FTO*	A	T	0.198	−0.0191	0.0196	0.328	1)	yes
rs1364063	16	68,146,073	*NFAT5*	T	C	0.864	−0.0236	0.0231	0.307	1)	no
rs9635759	17	46,968,784	*CA10*	A	G	0.435	0.0479	0.0172	0.005	1)	yes
rs1398217	18	43,006,236	*FUSSEL18*	G	C	0.599	−0.0225	0.0161	0.161	1)	yes
rs10423674	19	18,678,903	*CRTC1*	A	C	0.705	0.0031	0.0171	0.856	1)	yes
rs852069	20	17,070,593	*PCSK2*	A	G	0.776	−0.0340	0.0187	0.069	1)	yes

Genotyping result of 15,495 Japanese subjects were anlayzed in this study. Imputed SNPs with R2 of less than 0.7 were excluded from this analysis. A1 frequency of JPT were those from release 24 Hapmap JPT. N.D.; no data. References: 1 Elks et al Nat Genet 2010, 2 He et al Nature Genet 2009, 3 Liu et al Plos Genet 2009. P-value of 0.0015 (0.05/33) was set at the significant threshold for this candidate analysis.

*:Effect size and S.E. of allele1 on age at menarche (year per allele) and P-values were obtained by inverse-variance method.

**Concordance of association direction between this study and the previous report.

doi:10.1371/journal.pone.0063821.t004

uterine cervix, uterine body, ovary, hematopoietic organ), diabetes, myocardial infarction, brain infarction, arteriosclerosis, arrhythmia, drug eruption, liver cirrhosis, amyotrophic lateral sclerosis, osteoporosis, fibroid, and drug response, rheumatoid arthritis. chronic hepatitis B, pulmonary tuberculosis, keloid, heat cramp, brain aneurysm, chronic obstractive lung disease, glaucoma, and endometriosis (**Tables 1 and 2**). All subjects were collected under the support of the BioBank Japan Project [26], in which the individuals with any one of the 47 common diseases were enrolled between 2003 and 2008. Subjects under 17 years of age were not included in this study. Various life style information such as AAM was obtained through a face-to-face interview by trained medical coordinators using questionnaire sheets at each hospital. All participants provided written informed consent as

approved by the ethical committees of each institute. For participants between the age of 17 and 20 years old, we obtained written informed consent from both the participant and her parents. AAM was collected by self-report on the questionnaire. The subjects with AAM between the ages of 10 and 17 were enrolled for the study. This project was approved by the ethical committees of the BioBank Japan Project [26] and the University of Tokyo.

Genotyping and quality control

In the four GWAS enrolled in the meta-analysis of AAM, all samples were genotyped at more than 500,000 loci using one of the following platforms: Illumina HumanHap550v3 Genotyping BeadChip, Illumina HumanHap610-Quad Genotyping BeadChip, or Illumina Omni express Genotyping BeadChip (**Table 1**). Then we applied the following quality control for each GWAS separately: exclusion criteria; subjects with call rates<0.98, SNPs with call rates<0.99 or with ambiguous clustering of the intensity plots, or non-autosomal SNPs. We then excluded subjects whose ancestries were estimated to be distinct from East-Asian populations using principle component analysis performed by EIGENSTRAT version 2.0 [27]. Subsequently, the SNPs with MAF<0.01 or P-value of the Hardy-Weinberg equilibrium test$<1.0\times10^{-7}$ were excluded.

After the quality control criteria mentioned above were applied, genotype imputation was performed by MACH 1.0.16 [29] using the genotype data of Phase II HapMap JPT and CHB individuals (release 24)[28] as references, in a two-step procedure as described elsewhere [60]. In the first step of the imputation, recombination and error rate maps were estimated using 500 subjects randomly selected from the GWAS data. In the second step, imputation of the genotypes of all subjects was performed using the rate maps estimated in the first step. Quality control filters of MAF≥0.01 and *Rsq* values≥0.7 were applied for the imputed SNPs.

Statistical analysis

Associations of the SNPs with AAM were assessed by linear regression assuming the additive effects of the allele dosages on AAM, using mach2qtl software [29]. Years of birth and affection statuses of the diseases were used as covariates. Meta-analysis of all four GWAS was performed using an inverse-variance method from the summary statistics of beta and standard error (SE), using the Java source code implemented by the authors [61]. Genomic control correction was applied for each GWAS separately, and applied again for the results of GWAS meta-analysis. We set the P-values of 5.0×10^{-8} and 0.0015 (=0.05/33, Bonferroni's correction based on the numbers of the evaluated loci) as significance thresholds in GWAS and candidate gene analysis, respectively. Heterogeneity of the effect sizes among the studies was evaluated using Cochran's Q statistics.

Body mass index and Height QTL analysis

The associations of 42 SNPs with BMI and height were evaluated using previously published results, in which a total of 26,620 subjects with 32 diseases from Biobank Japan were enrolled [31]. Of the 26,620 subjects, 12,350 were also included in this AAM study. Genotyping was performed using the Illumina HumanHap610-Quad Genotyping BeadChip. Genotype imputation was performed using MACH 1.0. BMI was calculated based on self-reported body weight and height data. A rank-based inverse-normal transformation was applied to the BMI values of the subjects. Associations of the SNPs with transformed values of BMI were assessed by linear regression assuming additive effects of allele dosages (bound between 0.0 and 2.0) using mach2qtl software using gender, age, smoking history, the affection statuses of the diseases and the demographic classifications of the medical institutes in Japan where the subjects were enrolled were used as covariates.

Web resources

The URLs for data presented herein are as follows. BioBank Japan Project, http://biobankjp.org

MACH and mach2qtl software, http://www.sph.umich.edu/csg/abecasis/MACH/index.html International HapMap Project, http://www.hapmap.org PLINK software, http://pngu.mgh.harvard.edu/~purcell/plink/index.shtml EIGENSTRAT software, http://genepath.med.harvard.edu/~reich/Software.htm *R* statistical software, http://cran.r-project.org.

Supporting Information

Table S1 Age at menarche in each disease cohort.
(DOCX)

Table S2 The result of association analysis of TOP 42 SNPs from Japanese AAM study with body mass index and height from previous GWAS by Okada et al.
(DOCX)

Table S3 The result of top 42 SNPs by separated analysis.
(DOCX)

Acknowledgments

We would like to thank all the subjects who donated their DNA for this work. We also thank the technical staff of the Laboratory for Genotyping Development, Center for Genomic Medicine, RIKEN for their technical support.

Author Contributions

Conceived and designed the experiments: CT KO YN. Performed the experiments: CT AT NK MK. Analyzed the data: CT YO. Contributed reagents/materials/analysis tools: MK KM. Wrote the paper: CT YO YN KM.

References

1. Tena-Sempere M (2006) GPR54 and kisspeptin in reproduction. Hum Reprod Update 12: 631–639.
2. Susman EJ, Nottelmann ED, Inoff-Germain GE, Dorn LD, Cutler GB Jr, et al. (1985) The relation of relative hormonal levels and physical development and social-emotional behavior in young adolescents. Journal of Youth and Adolescence 14: 245–264.
3. Kaltiala-Heino R, Kosunen E, Rimpela M (2003) Pubertal timing, sexual behaviour and self-reported depression in middle adolescence. J Adolesc 26: 531–545.
4. Kaltiala-Heino R, Rimpela M, Rissanen A, Rantanen P (2001) Early puberty and early sexual activity are associated with bulimic-type eating pathology in middle adolescence. J Adolesc Health 28: 346–352.
5. Freedman DS, Khan LK, Serdula MK, Dietz WH, Srinivasan SR, et al. (2003) The relation of menarcheal age to obesity in childhood and adulthood: the Bogalusa heart study. BMC pediatrics 3: 3.
6. Kjaer K, Hagen C, Sandø S, Eshøj O (1992) Epidemiology of menarche and menstrual disturbances in an unselected group of women with insulin-dependent diabetes mellitus compared to controls. Journal of Clinical Endocrinology & Metabolism 75: 524–529.
7. Velie EM, Nechuta S, Osuch JR (2005) Lifetime reproductive and anthropometric risk factors for breast cancer in postmenopausal women. Breast Dis 24: 17–35.

8. Cooper GS, Ephross SA, Weinberg CR, Baird DD, Whelan EA, et al. (1999) Menstrual and reproductive risk factors for ischemic heart disease. Epidemiology 10: 255–259.
9. Fujiwara S, Kasagi F, Yamada M, Kodama K (1997) Risk factors for hip fracture in a Japanese cohort. Journal of Bone and Mineral Research 12: 998–1004.
10. Onland-Moret N, Peeters P, Van Gils C, Clavel-Chapelon F, Key T, et al. (2005) Age at menarche in relation to adult height. Am J Epidemiol 162: 623–632.
11. Anderson CA, Duffy DL, Martin NG, Visscher PM (2007) Estimation of variance components for age at menarche in twin families. Behav Genet 37: 668–677.
12. Towne B, Czerwinski SA, Demerath EW, Blangero J, Roche AF, et al. (2005) Heritability of age at menarche in girls from the Fels Longitudinal Study. American journal of physical anthropology 128: 210–219.
13. Treloar SA, Martin NG (1990) Age at menarche as a fitness trait: nonadditive genetic variance detected in a large twin sample. Am J Hum Genet 47: 137–148.
14. Anderson CA, Zhu G, Falchi M, Van Den Berg SM, Treloar SA, et al. (2008) A genome-wide linkage scan for age at menarche in three populations of European descent. Journal of Clinical Endocrinology & Metabolism 93: 3965.
15. Stavrou I, Zois C, Ioannidis JP, Tsatsoulis A (2002) Association of polymorphisms of the oestrogen receptor alpha gene with the age of menarche. Hum Reprod 17: 1101–1105.
16. Stavrou I, Zois C, Chatzikyriakidou A, Georgiou I, Tsatsoulis A (2006) Combined estrogen receptor alpha and estrogen receptor beta genotypes influence the age of menarche. Hum Reprod 21: 554–557.
17. Guo Y, Xiong DH, Yang TL, Guo YF, Recker RR, et al. (2006) Polymorphisms of estrogen-biosynthesis genes CYP17 and CYP19 may influence age at menarche: a genetic association study in Caucasian females. Hum Mol Genet 15: 2401–2408.
18. Xita N, Tsatsoulis A, Stavrou I, Georgiou I (2005) Association of SHBG gene polymorphism with menarche. Mol Hum Reprod 11: 459–462.
19. Rothenbuhler A, Fradin D, Heath S, Lefevre H, Bouvattier C, et al. (2006) Weight-adjusted genome scan analysis for mapping quantitative trait Loci for menarchal age. The Journal of clinical endocrinology and metabolism 91: 3534–3537.
20. Guo Y, Shen H, Xiao P, Xiong DH, Yang TL, et al. (2006) Genomewide linkage scan for quantitative trait loci underlying variation in age at menarche. The Journal of clinical endocrinology and metabolism 91: 1009–1014.
21. Elks CE, Perry JR, Sulem P, Chasman DI, Franceschini N, et al. (2010) Thirty new loci for age at menarche identified by a meta-analysis of genome-wide association studies. Nat Genet 42: 1077–1085.
22. Sulem P, Gudbjartsson DF, Rafnar T, Holm H, Olafsdottir EJ, et al. (2009) Genome-wide association study identifies sequence variants on 6q21 associated with age at menarche. Nat Genet 41: 734–738.
23. Ong KK, Elks CE, Li S, Zhao JH, Luan J, et al. (2009) Genetic variation in LIN28B is associated with the timing of puberty. Nature genetics 41: 729–733.
24. He C, Kraft P, Chen C, Buring JE, Pare G, et al. (2009) Genome-wide association studies identify loci associated with age at menarche and age at natural menopause. Nature genetics 41: 724–728.
25. Perry JR, Stolk L, Franceschini N, Lunetta KL, Zhai G, et al. (2009) Meta-analysis of genome-wide association data identifies two loci influencing age at menarche. Nat Genet 41: 648–650.
26. Nakamura Y (2007) The BioBank Japan Project. Clin Adv Hematol Oncol 5: 696–697.
27. Price AL, Patterson NJ, Plenge RM, Weinblatt ME, Shadick NA, et al. (2006) Principal components analysis corrects for stratification in genome-wide association studies. Nat Genet 38: 904–909.
28. The International HapMap Consortium (2003) The International HapMap Project. Nature 426: 789–796.
29. Li Y, Willer C, Sanna S, Abecasis G (2009) Genotype imputation. Annu Rev Genomics Hum Genet 10: 387–406.
30. Li J, Guo YF, Pei Y, Deng HW (2012) The impact of imputation on meta-analysis of genome-wide association studies. PLoS One 7: e34486.
31. Okada Y, Kubo M, Ohmiya H, Takahashi A, Kumasaka N, et al. (2012) Common variants at CDKAL1 and KLF9 are associated with body mass index in east Asian populations. Nat Genet 44: 302–306.
32. Okada Y, Sim X, Go MJ, Wu JY, Gu D, et al. (2012) Meta-analysis identifies multiple loci associated with kidney function-related traits in east Asian populations. Nat Genet 44: 904–909.
33. Okada Y, Hirota T, Kamatani Y, Takahashi A, Ohmiya H, et al. (2011) Identification of nine novel loci associated with white blood cell subtypes in a Japanese population. PLoS Genet 7: e1002067.
34. Okada Y, Kamatani Y, Takahashi A, Matsuda K, Hosono N, et al. (2010) A genome-wide association study in 19 633 Japanese subjects identified LHX3-QSOX2 and IGF1 as adult height loci. Hum Mol Genet 19: 2303–2312.
35. Okada Y, Kamatani Y, Takahashi A, Matsuda K, Hosono N, et al. (2010) Common variations in PSMD3-CSF3 and PLCB4 are associated with neutrophil count. Hum Mol Genet 19: 2079–2085.
36. He C, Kraft P, Chasman DI, Buring JE, Chen C, et al. (2010) A large-scale candidate gene association study of age at menarche and age at natural menopause. Human genetics 128: 515–527.
37. Kumar V, Kato N, Urabe Y, Takahashi A, Muroyama R, et al. (2011) Genome-wide association study identifies a susceptibility locus for HCV-induced hepatocellular carcinoma. Nat Genet In press.
38. Kumar V, Kato N, Urabe Y, Takahashi A, Muroyama R, et al. (2011) Genome-wide association study identifies a susceptibility locus for HCV-induced hepatocellular carcinoma. Nat Genet 43: 455–458.
39. Tanikawa C, Urabe Y, Matsuo K, Kubo M, Takahashi A, et al. (2012) A genome-wide association study identifies two susceptibility loci for duodenal ulcer in the Japanese population. Nat Genet In press.
40. Mbarek H, Ochi H, Urabe Y, Kumar V, Kubo M, et al. (2011) A genome-wide association study of chronic hepatitis B identified novel risk locus in a Japanese population. Hum Mol Genet 20: 3884–3892.
41. Urabe Y, Tanikawa C, Takahashi A, Okada Y, Morizono T, et al. (2012) A Genome-Wide Association Study of Nephrolithiasis in the Japanese Population Identifies Novel Susceptible Loci at 5q35. 3, 7p14. 3, and 13q14. 1. PLoS Genet 8: e1002541.
42. Cui R, Okada Y, Jang SG, Ku JL, Park JG, et al. (2011) Common variant in 6q26–q27 is associated with distal colon cancer in an Asian population. Gut 60: 799–805.
43. Ambros V, Horvitz HR (1984) Heterochronic mutants of the nematode Caenorhabditis elegans. Science 226: 409–416.
44. Heo I, Joo C, Cho J, Ha M, Han J, et al. (2008) Lin28 mediates the terminal uridylation of let-7 precursor MicroRNA. Molecular cell 32: 276–284.
45. Viswanathan SR, Daley GQ, Gregory RI (2008) Selective blockade of microRNA processing by Lin28. Science's STKE 320: 97.
46. Zhu H, Shah S, Shyh-Chang N, Shinoda G, Einhorn WS, et al. (2010) Lin28a transgenic mice manifest size and puberty phenotypes identified in human genetic association studies. Nat Genet 42: 626–630.
47. Guo Y, Chen Y, Ito H, Watanabe A, Ge X, et al. (2006) Identification and characterization of lin-28 homolog B (LIN28B) in human hepatocellular carcinoma. Gene 384: 51–61.
48. Yu J, Vodyanik MA, Smuga-Otto K, Antosiewicz-Bourget J, Frane JL, et al. (2007) Induced pluripotent stem cell lines derived from human somatic cells. Science 318: 1917–1920.
49. Gudbjartsson DF, Walters GB, Thorleifsson G, Stefansson H, Halldorsson BV, et al. (2008) Many sequence variants affecting diversity of adult human height. Nat Genet 40: 609–615.
50. Lettre G, Jackson AU, Gieger C, Schumacher FR, Berndt SI, et al. (2008) Identification of ten loci associated with height highlights new biological pathways in human growth. Nat Genet 40: 584–591.
51. Krude H, Schutz B, Biebermann H, Von Moers A, Schnabel D, et al. (2002) Choreoathetosis, hypothyroidism, and pulmonary alterations due to human NKX2-1 haploinsufficiency. Journal of Clinical Investigation 109: 475–480.
52. Eriksson N, Benton GM, Do CB, Kiefer AK, Mountain JL, et al. (2012) Genetic variants associated with breast size also influence breast cancer risk. BMC Med Genet 13: 53.
53. Bhalla K, Luo Y, Buchan T, Beachem MA, Guzauskas GF, et al. (2008) Alterations in CDH15 and KIRREL3 in patients with mild to severe intellectual disability. Am J Hum Genet 83: 703–713.
54. Guerin A, Stavropoulos DJ, Diab Y, Chénier S, Christensen H, et al. (2012) Interstitial deletion of 11q-implicating the KIRREL3 gene in the neurocognitive delay associated with Jacobsen syndrome. American Journal of Medical Genetics Part A.
55. Elks CE, Perry JR, Sulem P, Chasman DI, Franceschini N, et al. (2010) Thirty new loci for age at menarche identified by a meta-analysis of genome-wide association studies. Nat Genet 42: 1077–1085.
56. Melzer D, Perry JR, Hernandez D, Corsi AM, Stevens K, et al. (2008) A genome-wide association study identifies protein quantitative trait loci (pQTLs). PLoS Genet 4: e1000072.
57. Yazawa M, Ferrante C, Feng J, Mio K, Ogura T, et al. (2007) TRIC channels are essential for Ca2+ handling in intracellular stores. Nature 448: 78–82.
58. Volodarsky M, Markus B, Cohen I, Staretz-Chacham O, Flusser H, et al. (2013) A Deletion Mutation in TMEM38B Associated with Autosomal Recessive Osteogenesis Imperfecta. Hum Mutat.
59. Parent AS, Teilmann G, Juul A, Skakkebaek NE, Toppari J, et al. (2003) The timing of normal puberty and the age limits of sexual precocity: variations around the world, secular trends, and changes after migration. Endocr Rev 24: 668–693.
60. Okada Y, Takahashi A, Ohmiya H, Kumasaka N, Kamatani Y, et al. (2011) Genome-wide association study for C-reactive protein levels identified pleiotropic associations in the IL6 locus. Hum Mol Genet 20: 1224–1231.
61. Yamaguchi-Kabata Y, Nakazono K, Takahashi A, Saito S, Hosono N, et al. (2008) Japanese population structure, based on SNP genotypes from 7003 individuals compared to other ethnic groups: effects on population-based association studies. The American Journal of Human Genetics 83: 445–456.

OPEN ACCESS Freely available online

PLOS ONE

Antitumor Activity and Induction of TP53-Dependent Apoptosis toward Ovarian Clear Cell Adenocarcinoma by the Dual PI3K/mTOR Inhibitor DS-7423

Tomoko Kashiyama[1], Katsutoshi Oda[1]*, Yuji Ikeda[1], Yoshinobu Shiose[2], Yasuhide Hirota[2], Kanako Inaba[1], Chinami Makii[1], Reiko Kurikawa[1], Aki Miyasaka[1], Takahiro Koso[1], Tomohiko Fukuda[1], Michihiro Tanikawa[1], Keiko Shoji[1], Kenbun Sone[1], Takahide Arimoto[1], Osamu Wada-Hiraike[1], Kei Kawana[1], Shunsuke Nakagawa[3], Koichi Matsuda[4], Frank McCormick[5], Hiroyuki Aburatani[6], Tetsu Yano[7], Yutaka Osuga[1], Tomoyuki Fujii[1]

1 Department of Obstetrics and Gynecology, Faculty of Medicine, The University of Tokyo, Tokyo, Japan, **2** Oncology Research Laboratories, Daiichi Sankyo Co. Ltd., Tokyo, Japan, **3** Department of Obstetrics and Gynecology, Faculty of Medicine, Teikyo University, Tokyo, Japan, **4** Laboratory of Molecular Medicine, Human Genome Center, Institute of Medical Science, The University of Tokyo, Tokyo, Japan, **5** Helen Diller Family Comprehensive Cancer Center, University of California San Francisco, San Francisco, California, United States of America, **6** Genome Science Division, Research Center for Advanced Science and Technology, The University of Tokyo, Tokyo, Japan, **7** Department of Obstetrics and Gynecology, National Center for Global Health and Medicine, Tokyo, Japan

Abstract

DS-7423, a novel, small-molecule dual inhibitor of phosphatidylinositol-3-kinase (PI3K) and mammalian target of rapamycin (mTOR), is currently in phase I clinical trials for solid tumors. Although DS-7423 potently inhibits PI3Kα (IC_{50} = 15.6 nM) and mTOR (IC_{50} = 34.9 nM), it also inhibits other isoforms of class I PI3K (IC_{50} values: PI3Kβ = 1,143 nM; PI3Kγ = 249 nM; PI3Kδ = 262 nM). The PI3K/mTOR pathway is frequently activated in ovarian clear cell adenocarcinomas (OCCA) through various mutations that activate PI3K-AKT signaling. Here, we describe the anti-tumor effect of DS-7423 on a panel of nine OCCA cell lines. IC_{50} values for DS-7423 were <75 nM in all the lines, regardless of the mutational status of *PIK3CA*. In mouse xenograft models, DS-7423 suppressed the tumor growth of OCCA in a dose-dependent manner. Flow cytometry analysis revealed a decrease in S-phase cell populations in all the cell lines and an increase in sub-G1 cell populations following treatment with DS-7423 in six of the nine OCCA cell lines tested. DS-7423-mediated apoptosis was induced more effectively in the six cell lines without *TP53* mutations than in the three cell lines with *TP53* mutations. Concomitantly with the decreased phosphorylation level of MDM2 (mouse double minute 2 homolog), the level of phosphorylation of TP53 at Ser46 was increased by DS-7423 in the six cell lines with wild-type *TP53*, with induction of genes that mediate TP53-dependent apoptosis, including *p53AIP1* and *PUMA* at 39 nM or higher doses. Our data suggest that the dual PI3K/mTOR inhibitor DS-7423 may constitute a promising molecular targeted therapy for OCCA, and that its antitumor effect might be partly obtained by induction of TP53-dependent apoptosis in *TP53* wild-type OCCAs.

Citation: Kashiyama T, Oda K, Ikeda Y, Shiose Y, Hirota Y, et al. (2014) Antitumor Activity and Induction of TP53-Dependent Apoptosis toward Ovarian Clear Cell Adenocarcinoma by the Dual PI3K/mTOR Inhibitor DS-7423. PLoS ONE 9(2): e87220. doi:10.1371/journal.pone.0087220

Editor: Yuan-Soon Ho, Taipei Medical University, Taiwan

Received September 30, 2013; **Accepted** December 18, 2013; **Published** February 4, 2014

Funding: This work was supported by Daiichi Sankyo Co. Ltd., The Grant-in-Aid for Scientific Research (C), Grant Number 19599005 and 23592437 from the Ministry of Education, Culture, Sports, Science and Technology of Japan (to K Oda). This study was also performed as a research program of the Project for Development of Innovative Research on Cancer Therapeutics (P-Direct), Ministry of Education, Culture, Sports, Science and Technology of Japan (to T Yano). Yoshinobu Shiose and Yasuhide Hirota, employees of Daiichi Sankyo Co. Ltd, contributed to the experiments (in vivo experiments) as listed in the "contributions" of each author. The funders themselves had no role in study design, data collection and analysis, decision to publish, or preparation of the manuscript.

Competing Interests: Yoshinobu Shiose and Yasuhide Hirota are employees of Daiichi Sankyo Co. Ltd, which partly supported this work (to K Oda). DS-7423 is in clinical development by Daiichi Sankyo Co. Ltd and was provided by the company for use in this study. There are no other relevant COI related to employment, consultancy, patents, products in development, or marketed products. These COI do not alter the authors' adherence to all the PLOS ONE policies on sharing data and materials.

* E-mail: katsutoshi-tky@umin.ac.jp

Introduction

The phosphatidylinositol 3-kinase (PI3K)-AKT signaling pathway is frequently activated in various types of cancers, and several inhibitors that target this pathway have been developed as potential cancer therapeutics. The constitutive activation of the PI3K-AKT pathway results from various types of alterations, including the overexpression of receptor tyrosine kinases (RTKs), as well as mutations of *Ras*, the catalytic subunit p110α of phosphoinositide-3-kinase (*PIK3CA*), and *PTEN* [1]. Class I PI3Ks include four isoforms of the catalytic subunit (p110α, p110β, p110γ, and p110δ). Among these four isoforms, p110α is broadly mutated and predominantly activated in various types of human cancers, although p110β and p110δ might be selectively activated in certain tumors such as those with loss of PTEN function [2,3]. Mammalian target of rapamycin (mTOR) is the catalytic subunit found in two distinct complexes: the raptor-containing complex mTORC1 and the rictor-containing complex mTORC2 [4]. AKT activates mTORC1 signaling and also phosphorylates other downstream proteins, including GSK3β, forkhead box-O tran-

scription factors (FOXOs), and mouse double minute 2 homolog (MDM2) [5]. mTORC1 controls protein synthesis and cell proliferation via the phosphorylation of its downstream targets, 4E-BP1 and S6 kinase 1 (S6K1) [6]. Rapamycin and its analogs (rapalogs) block mTORC1 activity, but not mTORC2 activity [7]. One of the AKT downstream targets, MDM2, is a negative regulator of TP53 that induces its ubiquitination and subsequent degradation [8]. Although the cytostatic effects of PI3K pathway inhibitors have been reported in various types of cancers [9–12], targeting the PI3K pathway might induce cytotoxic effects by suppressing anti-apoptotic signals through the dephosphorylation of FOXOs and stabilization of TP53. It seems reasonable to suspect that targeting the PI3K-mTOR axis might be a promising therapeutic strategy to selectively induce apoptosis of cancer cells, especially those without mutations in *TP53*.

Epithelial ovarian cancer is a leading cause of death resulting from gynecological malignancies. Ovarian clear cell adenocarcinoma (OCCA) is the second most common cause of death from ovarian cancer, with a higher incidence in Asia, especially in Japan (>25%), than in other continents [13]. OCCA is derived primarily from ovarian endometriosis, and the clinical outcome is generally poor, owing to low response rates to conventional platinum-based chemotherapy [14]. Thus, novel therapeutic strategies are warranted to improve the clinical outcome of OCCA. In histological terms, ovarian serous adenocarcinoma (OSA) is the most common variant of ovarian carcinoma [15]. It is highly sensitive to platinum-based chemotherapy, with a primary clinical response rate of >70%. The mutational spectrum differs between OCCA and OSA, with *TP53* mutations observed in almost all (96%) OSA tumors, but in only 10% of OCCA tumors [15,16]. In particular, mutations of *RB1* and *BRCA1/2* are much more common in OSA than in OCCA. However, *PIK3CA* mutations are more frequent in OCCA (>40%) than in OSA (<10%) [17]. Although mutations of *KRAS* and *PTEN* are rare (<10%), the overexpression of several RTKs has been reported in OCCA, including human epidermal growth factor receptor 2 (HER2) with a frequency of approximately 40% and cMET with a frequency of approximately 30% [18–21]. Taken together, these observations suggest that the RTK-PI3K/mTOR signaling axis might be broadly activated in OCCA.

DS-7423 is a novel, small-molecule compound that inhibits both PI3K and mTOR (mTORC1/2). It inhibits all class I PI3K isoforms with greater potency against p110α than against the other p110 isoforms. Relevant activity (IC_{50} <200 nM) was not observed in any of the 227 kinases tested, except for Mixed Lineage Kinase 1 (MLK1) and Never-In-Mitosis Gene A (NIMA)-related kinase 2 (NEK2). The compound is currently in phase I clinical trials for solid tumors. In this study, we evaluated its anti-tumor efficacy in a panel of OCCA cell lines. We focused in particular on the ability of DS-7423 to induce apoptosis, and on whether the apoptosis might be mediated by TP53.

Materials and Methods

Small-molecule compounds

The small molecule compound DS-7423 was provided by the Daiichi-Sankyo Company, Ltd (Tokyo, Japan). The drug information about DS-7423 is available on the ClinicalTrials.gov website (NCT01364844). The mTOR inhibitor rapamycin was purchased from Cayman Chemical (Michigan, USA).

Cell lines

The OVTOKO, OVISE, OVMANA, RMG-I, OVSAHO, OVKATE, and OV1063 lines were purchased from the Japanese Collection of Research Bioresources (JCRB) Cell Bank (Osaka, Japan). The JHOC-7, JHOC-9, HTOA, JHOS-2, JHOS-3, and JHOS-4 cell lines were purchased from the RIKEN Cell Bank (Ibaraki, Japan). The TOV-21, ES-2, and SKOV3 cell lines were from the American Type Culture Collection (Manassas, VA). OVISE, OVTOKO, TOV-21G and ES2 were cultured in RPMI1640 medium containing 10% fetal bovine serum (FBS). OVMANA was cultured in RPMI medium containing 20% FBS, JHOC-7 in DMEM/F12 medium containing 10% FBS, JHOC-9 and RMG-I in DMEM/F12 medium containing 20% FBS, and SKOV3 in DMEM containing 10% FBS. The OVSAHO, OVKATE, OV1063, HTOA, JHOS-2, JHOS-3, and JHOS-4 lines were cultured in DMEM medium containing 10% FBS. The histological subtype of the SKOV3 cells was not unambiguously defined even after extensive analysis, although it was confidently identified as clear cell adenocarcinoma [22]. The immortalized epithelial cell line from an ovarian endometrial cyst was a generous gift from Dr. Satoru Kyo [23].

Polymerase chain reaction (PCR) and sequencing

The mutational status of all nine OCCA cell lines was analyzed by PCR and direct sequencing. The PCR conditions and primers for the analysis of *PTEN* (exons 1–9) and *K-Ras* (exon 1 and 2) sequences were described previously [24–26]. The entire coding region of *PIK3CA* was analyzed by reverse transcription (RT)-PCR with LA-Taq according to the manufacturer's protocol (Takara BIO, Madison, WI) [27]. The PCR primers for analysis of *TP53* (exons 4–8) were described previously [28].

Proliferation assays

Assays of the suppression of cell proliferation were performed with the Cell Counting Kit-8 using the tetrazolium salt WST-8 [2-(2-methoxy-4-nitrophenyl)-3-(4-nitrophenyl)-5-(2,4-disulfophenyl)-2H-tetrazolium, monosodium salt] (Dojindo, Tokyo, Japan) for the methyl thiazolyl tetrazolium (MTT) assay. Using 96-well plates, 2,000 cells were seeded on the appropriate medium and treated with increasing doses (0–2,500 nM) of DS-7423 or rapamycin for 72 h, starting from 24 h after seeding. Proliferation was quantified by monitoring the changes in the absorbance at 450 nm, which were normalized relative to the absorbance of cell cultures treated with DMSO alone.

Immunoblotting

Cells were treated with DS-7423 or rapamycin for the indicated time and at the indicated concentration, and were then lysed in the cell lysis buffer (Cell Signaling Technology, Beverly, MA). Antibodies to total Akt, phosphorylation of Akt (p-Akt) (Ser473, Thr308), p-GSK3beta (Ser9), total S6, p-S6 (Ser235/236, Ser 240/244), p-4EBP1 (Thr37/46), p-FOXO1 (Thr24), p-FOXO3a (Thr32), p-MDM2 (Ser 166), p-TP53 (Ser15), cleaved-PARP, and PARP (Cell Signaling Technology, Beverly, MA), beta-actin (Sigma-Aldrich, St. Louis, MO), TP53 (Santa Cruz, CA, USA) and p-TP53 (Ser46) (Calbiochem, Billerica, MA) were used for immunoblotting, as recommended by the manufacturers. Signals were detected using BioRAD western blotting systems (BioRAD, Hercules, CA) with the detection reagents ECL advance and ECL select (GE Healthcare, Piscataway, NJ).

Cell cycle analysis

Cells (5×10^5) were seeded in 60-mm dishes and treated with DS-7423 for 48 h. Floating and adherent cells were collected by trypsinization and washed twice with phosphate buffer saline (PBS). Cells were resuspended in cold 70% ethanol and

maintained at 4°C overnight. After being washed twice with PBS, cells were incubated in RNase A (0.25 mg/mL) (Sigma) for 30 min at 37°C, followed by staining with propidium iodide (PI; 50 μg/mL) (Sigma) at 4°C for 30 min in the dark. Cells were then analyzed using flow cytometry (BD FACS Calibur HG, Franklin Lakes, NJ). Cell cycle distribution was analyzed using CELL Quest pro ver. 3.1. (Beckman Coulter Epics XL, Brea, CA). All experiments were repeated three times.

Detection of apoptosis by staining with annexin-V FITC

Cells (5×10^5) were cultured in 60-mm plates for 24 h before treatment with either DMSO (control), and 156 nM DS-7423, or 2,500 nM DS-7423 for 48 h. Cells were trypsinized, washed twice with PBS, and then analyzed after double staining with annexin-V fluorescein isothiocyanate (FITC) (Abcam, Cambridge, MA) and PI. The apoptotic cell population was analyzed using flow cytometry. All experiments were performed three times.

Ethics statement for animal experiments

This study was approved by Animal Care and Use Committee, Daiichi-Sankyo Pharmaceutical Co. Ltd. Athymic mice were maintained in an SPF (Specific Pathogen Free) facility according to our institutional guidelines, and experiments were conducted under an approved animal protocol.

Tumor xenografts in nude mice

Specific pathogen-free female nude mice (BALB/cAJcl-nu/nu), 6 weeks old, were purchased from CLEA Japan, Inc (Tokyo, Japan). Subcutaneous xenograft tumors in the mice were established by the injection of a 100-μL suspension containing 5×10^6 cells of the TOV-21, RMG-I, or ES-2 lines in PBS. Tumors were removed after exponential growth, cut into 3-mm pieces, and transplanted subcutaneously into other mice for RMG-I cells. DS-7423 was suspended in 0.5 w/v% Methyl Cellulose 400 solution (Wako Pure Chemical Industries, Ltd.) Oral daily administration of DS-7423 started 8–22 days later, following the injection of the cells ($5–6\times10^6$ cells/0.1 mL). One week after tumor transplantation, mice were assigned randomly to one of the three treatment regimens: (1) non-treated control, (2) DS-7423 (1.5 mg/kg), (3) DS-7423 (3 mg/kg), and (4) DS-7423 (6 mg/kg). Each treatment group consisted of five mice. DS-7423 was injected orally (p.o.) once a day. Tumor volumes (in mm^3) were calculated by the formula: ([major axis] × [minor axis]^2/2). After the treatment, the tumors were removed and analyzed by western blotting. Tumor weight (wet weight) was measured, and the average weight was calculated for each group.

Semi-quantitative RT-PCR analysis

OCCA cells were treated with either DMSO or the indicated concentration of either DS-7423 or rapamycin for 24 h. Total RNAs of these cells were extracted with the RNeasy Mini Kit according to the manufacturer's instructions (QIAGEN, Valencia, CA). cDNAs were synthesized from total RNAs by using the Super Script III First-strand Synthesis SuperMix (Invitrogen, Carlsbad, CA). The exponential phase of the RT-PCR occurred between 15–30 cycles, and these cycles were monitored to allow semi-quantitative comparisons among the cDNAs developed from identical reactions. The primers and conditions for the amplification of *p53AIP1*, *p21*, and *GAPDH* sequences were described previously [29]. The PCR primers for *PUMA* were 5′-TGAGACAAGAGGAGCAGCAG-3′ (forward) and 5′-ACCTAATTGGGCTCCAT CTC-3′ (reverse). The primers for p53R2, TIGAR, GLS2, GADD45, 14-3-3 sigma and PAI-1 were described previously [30–35]. Each PCR regimen involved a 2-min initial denaturation step (94°C), which was followed by 15–30 cycles at 94°C for 30 s, then at 55°C for 30 s, and finally, at 72°C for 30 s using a Thermal Cycler Gene Atlas instrument (ASTEC, Fukuoka, Japan).

Gene silencing

Cells were plated at approximately 30% confluence in 100-mm plates and incubated for 24 h before transfection with small interfering RNA (siRNA) duplexes at the concentrations indicated, using Lipofectamine 2000 RNAiMAX (Invitrogen, Carlsbad, CA) and Opti-MEM medium (Life Technologies, Grand Island, NY). The siRNAs specific for TP53 were purchased from Invitrogen. A negative control kit was used as a control (Invitrogen, Carlsbad, CA).

Luciferase assay

Transfection was performed using Effectene reagent (QIAGEN, Valencia, CA) according to the manufacturer's recommendation. The TP53 expression plasmid (0.1 μg/μL) was cotransfected with pp53 TA Luc (0.25 μg/mL). The phRL CMV-Renilla plasmid (Promega, Madison, WI) was also transfected in all experiments as the internal control to normalize the transfection efficiency. The assays, each involving triplicate wells, were repeated three times.

Statistical analysis

The data were expressed as means ± standard deviations of three independent determinations. The significance of the difference between two samples was analyzed using the Student's t-test, and a p-value of <0.05 was considered to denote a statistically significant difference.

Results

Genetic alterations and activation of the PI3K-AKT signaling pathway in OCCA cell lines

We evaluated the phosphorylation (p-) levels of the proteins in the PI3K-AKT pathway by using an immortalized epithelial cell line from an ovarian endometrial cyst as a control. AKT was phosphorylated at Thr308 in seven of the nine OCCA cell lines tested (Figure 1). The cell lines OVMANA and ES-2 had low levels of p-AKT (Thr308) (Figure 1). The phosphorylation levels of S6, 4E-BP1 and/or FOXO1/3a, the downstream targets of AKT, were upregulated in the OCCA cells, including OVMANA and ES-2.

Four of the nine cell lines possessed *PIK3CA* mutations (44%) (Figure 1 and Table S1), and one of these four, TOV-21G, also possessed mutations in *PTEN* and *K-Ras* (11%). *TP53* mutations were detected in three cell lines (33%) (Table S1). The mutational status of *PIK3CA* was not associated with the phosphorylation of AKT or proteins that act downstream of AKT. Next, the expression and phosphorylation levels of three RTKs (HER2, HER3, and MET), which have been reported to be overexpressed in OCCA, were evaluated. The levels of phosphorylation of both HER2 (Tyr1221/1222) and HER3 (Tyr1289) were correlated with the abundances of these two proteins (Figure 1). p-HER2 and p-HER3 levels were elevated in four (44%: OVISE, SKOV3, JHOC7 and RMG-I) and six (67%: TOV-21G, OVISE, OVMANA, OVTOKO, JHOC-7 and RMG-I) cell lines, respectively (Figure 1). The expression of MET was higher in all nine OCCA cell lines than in the control, although the level of p-MET was increased in only two cell lines (22%: JHOC-7 and RMG-I). Taken together, all the OCCA cell lines, except for ES-2 and JHOC-9, possessed one or more activating alterations in the RTK-PI3K genes examined (Figure 1 and Table S1). Each of the

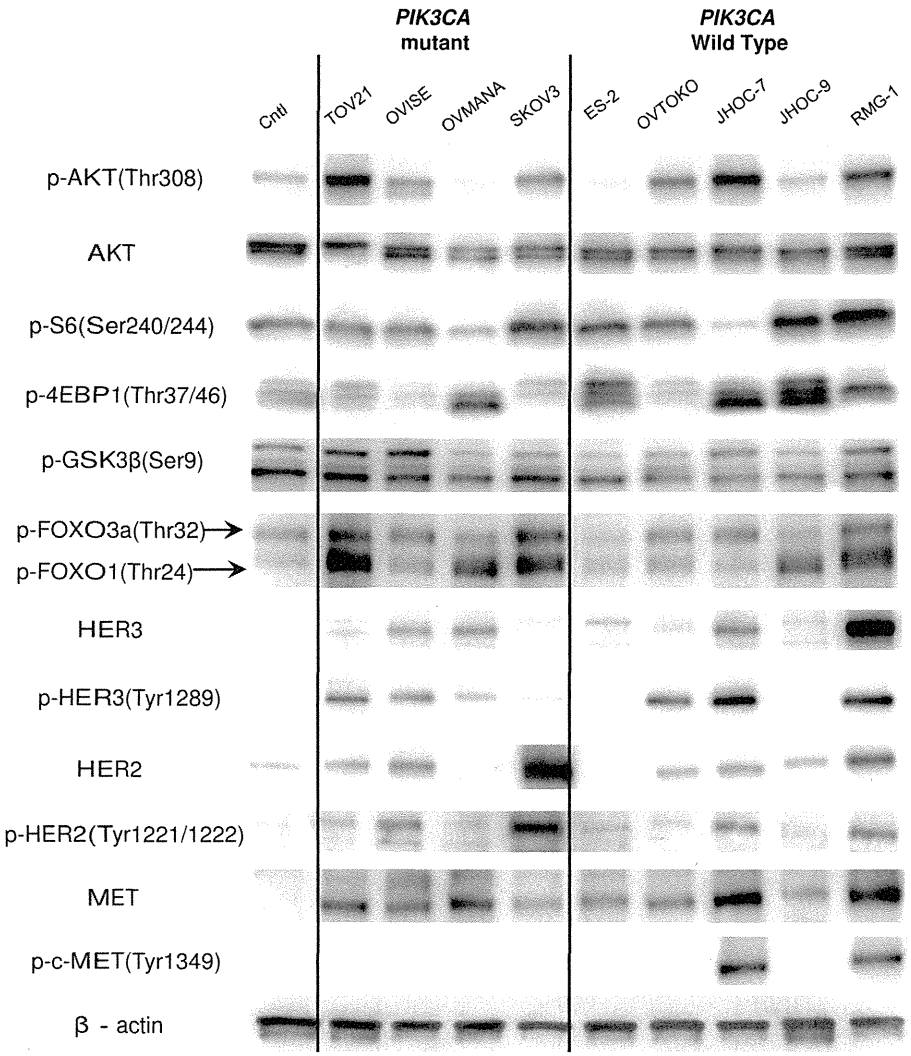

Figure 1. Phosphorylation and mutational status of genes that encode components of the RTK/Ras/PI3K pathway. Nine ovarian clear cell adenocarcinoma (OCCA) and a control (Cntl) cell line (immortalized epithelial cells from ovarian endometrioma) were lysed in cell lysis buffer and analyzed by western blotting. In general, most of the OCCA cell lines displayed higher levels of phosphorylation of Akt (Thr308) and its downstream targets (GSK3β, FOXO 1/3a, 4EBP1 and S6) than the respective levels of phosphorylation in the control line. The abundances and levels of phosphorylation of c-MET (Tyr1234/1235), HER2 (Tyr1221/1222), and HER3 (Tyr1289) were also evaluated. The mutational status of *PIK3CA*, *PTEN*, and *K-Ras* is shown for each cell line.
doi:10.1371/journal.pone.0087220.g001

four cell lines with *PIK3CA* mutations showed concomitant activation of RTKs, defined as high levels of phosphorylation of HER2 and/or HER3.

Anti-proliferative effect of DS-7423 in OCCA cell lines

We tested the anti-proliferative effects of the dual PI3K/mTOR inhibitor, DS-7423, and the mTOR (mTORC1) inhibitor, rapamycin, in each of the nine OCCA cell lines. Exposure to 156 nM DS-7423 inhibited cell growth by 70%–97%, and the IC_{50} values for cell proliferation were 20–75 nM (Figure 2A). Dose-dependent growth suppression was more clearly induced by DS-7423 than by rapamycin in each of the nine cell lines (Figure 2A). The IC_{50} value was not reached with rapamycin at any of the concentrations tested (2.45–2,560 nM) in five (OVMANA, SKOV3, OVTOKO, JHOC-7 and RMG-I) of the nine OCCA cell lines. We also examined the effect of DS-7423 in seven OSA lines. The IC_{50} values with DS-7423 were >100 nM in four of these seven OSAs (Figure 2B). The ratio of resistant cell lines (IC_{50} >100 nM) was significantly higher in OSA cell lines (57%) than in OCCA cell lines (0%) ($p = 0.019$ by Fisher's exact test).

We performed immunoblotting on the lysates prepared from the cells treated with DS-7423 or rapamycin. DS-7423 suppressed the phosphorylation of AKT (Thr308 and Ser473) and S6 (Ser235/236 and Ser240/244) at doses of 39–156 nM and higher (Figure 3A and Figure S1). DS-7423 suppressed the phosphorylation levels of the targeted proteins at comparable doses in the AKT pathway (AKT, FOXO1/3a, and MDM2) and mTORC1 pathway (S6). Rapamycin did not suppress p-Akt at any dose, and suppressed p-S6 at 2.45 nM or higher doses (Figure 3B). On the

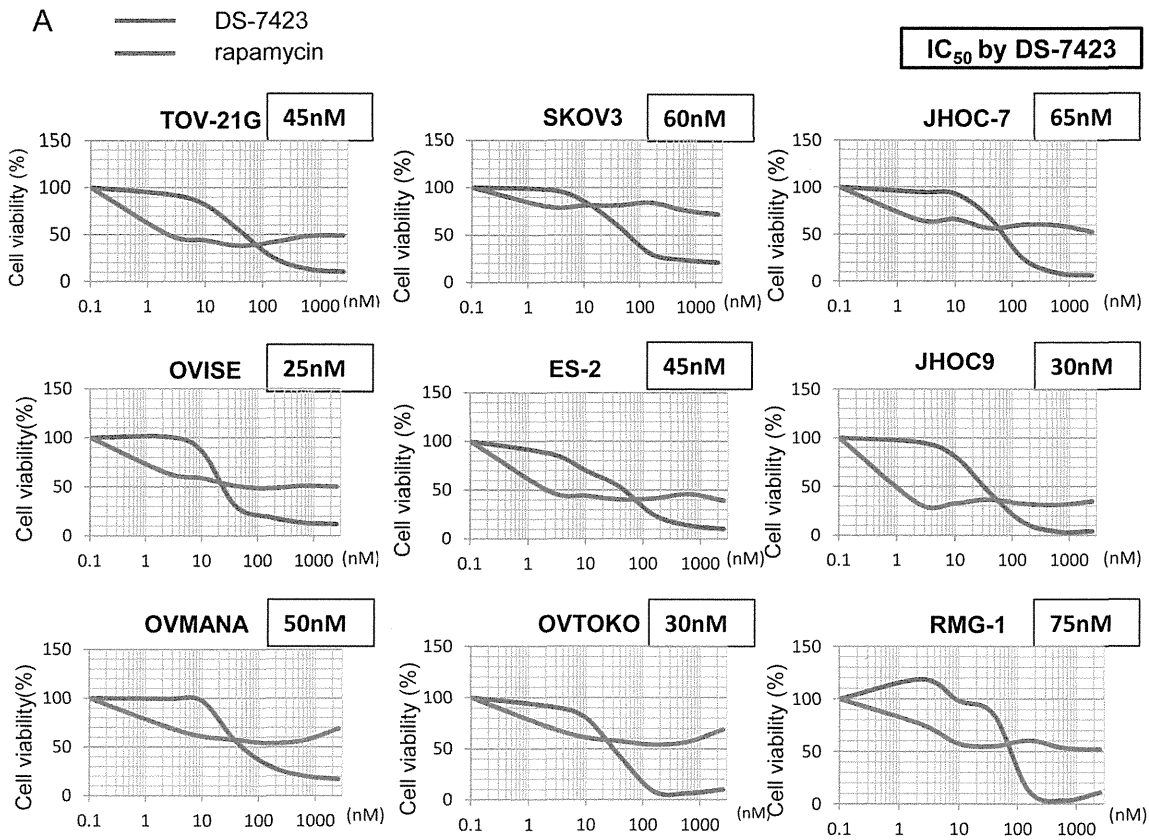

B

OSA	IC_{50} (nM)
JHOS-3	45
HTOA	60
OVSAHO	65
JHOS-4	120
JHOS-2	250
OV1063	700
OVKATE	>2,500

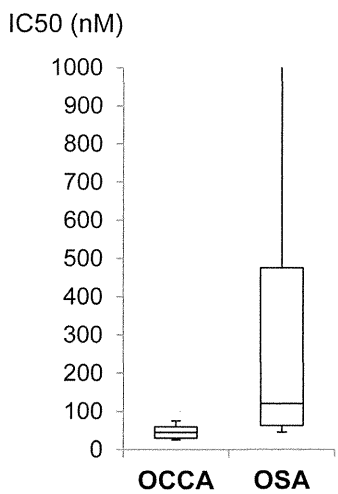

Figure 2. Inhibition of cell proliferation by DS-7423 and rapamycin. (A) Cell viability for each cell line was analyzed using the methyl thiazolyl tetrazolium (MTT) assay 72 h after treatment with DS-7423 or rapamycin at the doses indicated. The data were normalized relative to the value of the control cells. In all nine cell lines, DS-7423 suppressed cell proliferation more robustly than rapamycin when both were used at higher doses. (B) IC_{50} values for DS-7423 in seven ovarian serous adenocarcinoma (OSA) cell lines (left) were compared with those of nine OCCA cells (right). Four of seven OSA cells had IC_{50} values >100 nM, which is higher than that of any OCCA cells.
doi:10.1371/journal.pone.0087220.g002

contrary, rapamycin increased the levels of p-FOXO3a and p-FOXO1 at 2,500 nM (Figure 3B).

We conducted fluorescence-activated cell sorting (FACS)-based cell cycle analyses in OCCA cells treated with DS-7423. DS-7423 decreased the size of the S-phase population in the

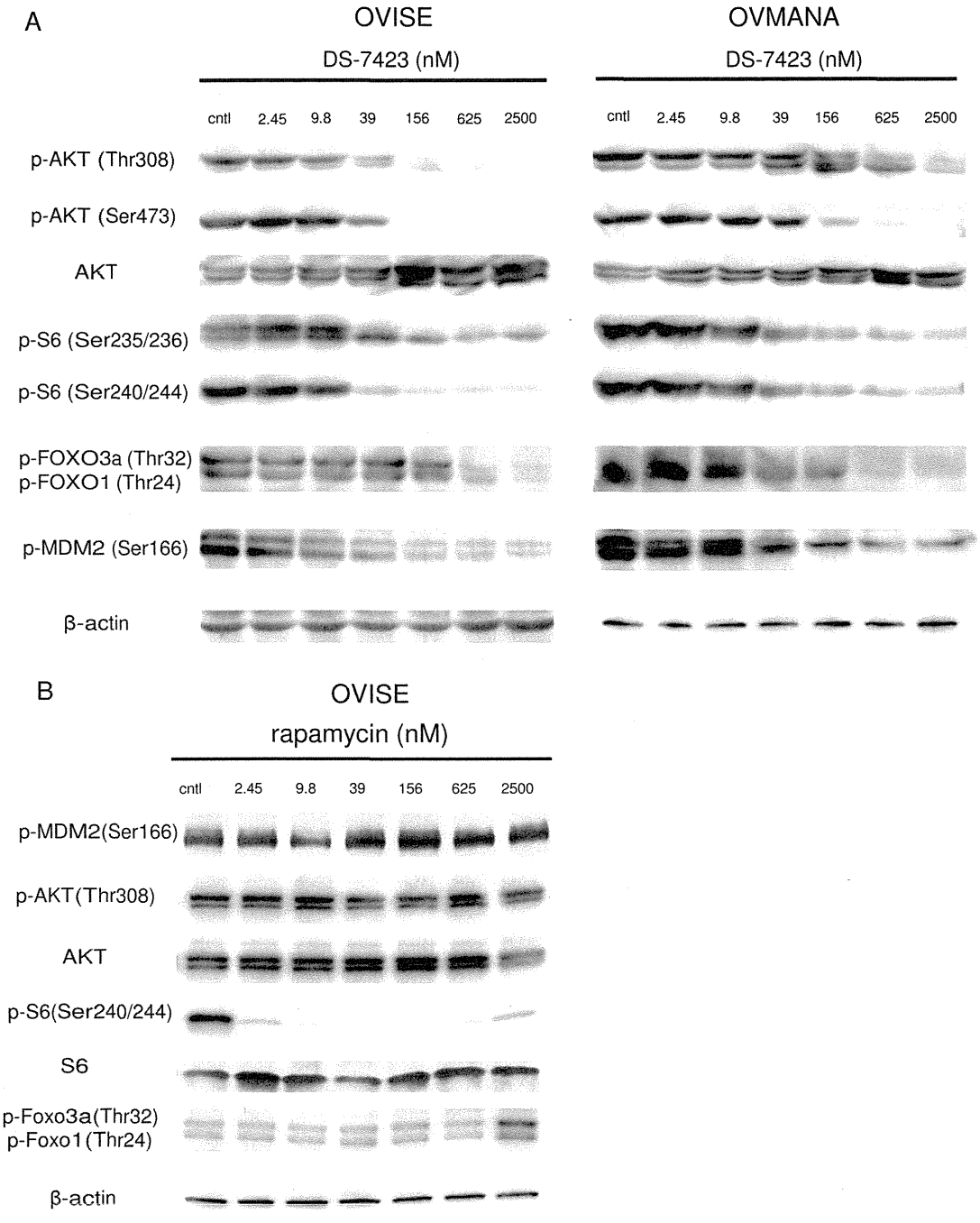

Figure 3. Inhibition of PI3K/mTOR signaling by DS-7423 and rapamycin in ovarian clear cell adenocarcinoma cell lines. (A) Immunoblotting of total protein extracts from OCCA cells (OVISE and OVMANA) treated with DS-7423 at concentrations ranging from 0 to 2,500 nM. (B) Immunoblotting of total protein extracts from OVISE cells treated with rapamycin at concentrations ranging from 0 to 2,500 nM.
doi:10.1371/journal.pone.0087220.g003

OCCA cells, although the change was weak in ES-2 cells. (Figure 4A). G1 arrest was predominantly observed in six of the nine cell lines. The sizes of sub-G1 populations increased in a dose-dependent manner in six of the nine cell lines, especially in OVISE and OVMANA cells.

In vivo antitumor effect of DS-7423 in a mouse xenograft model

In vivo antitumor activity of DS-7423 in mice implanted with either TOV-21G cells or RMG-1 tumor pieces was examined. Oral daily administration of DS-7423 significantly suppressed the tumor growth of the xenografts of TOV-21G and RMG-I in a

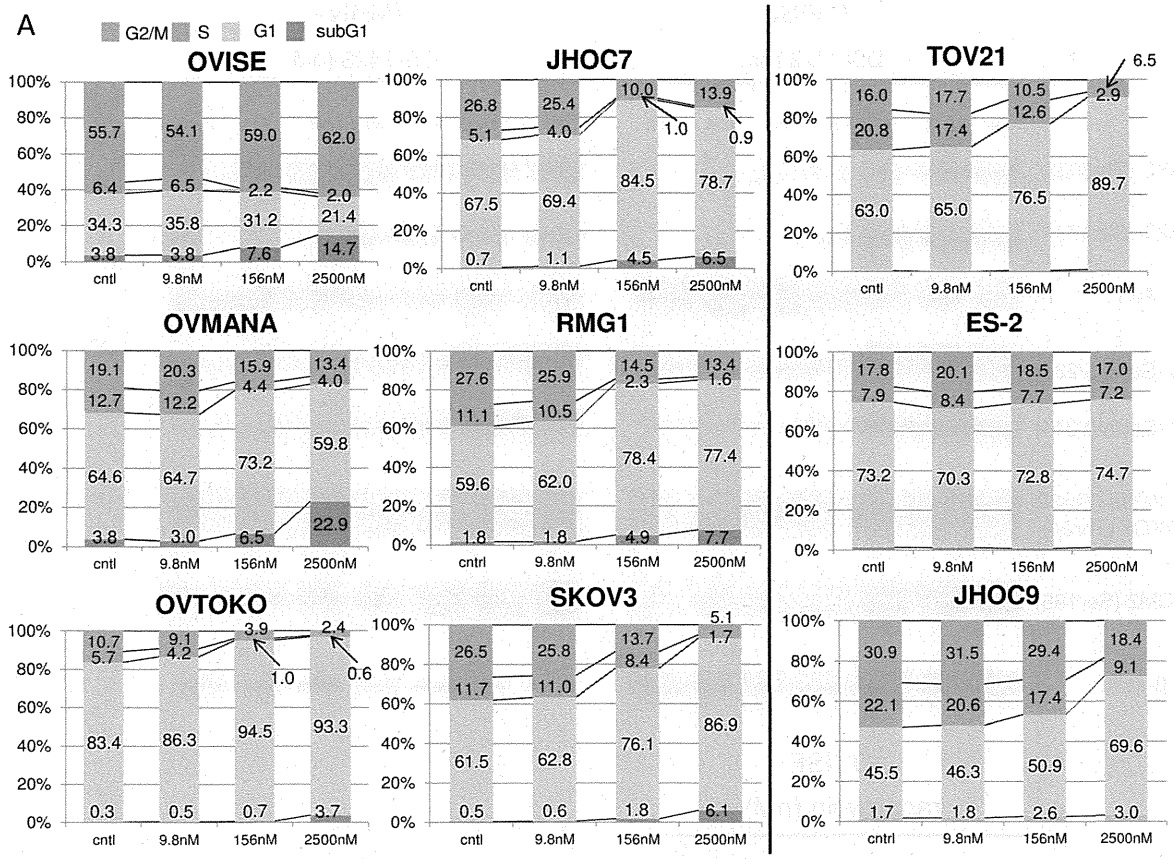
A
G2/M
S
G1
subG1
OVISE
JHOC7
TOV21
OVMANA
RMG1
ES-2
OVTOKO
SKOV3
JHOC9
100%
80%
60%
40%
20%
0%
cntl
9.8nM
156nM
2500nM
55.7
54.1
59.0
62.0
6.4
6.5
2.2
2.0
34.3
35.8
31.2
21.4
3.8
3.8
7.6
14.7
26.8
25.4
10.0
13.9
5.1
4.0
1.0
0.9
67.5
69.4
84.5
78.7
0.7
1.1
4.5
6.5
16.0
17.7
10.5
2.9
6.5
20.8
17.4
12.6
63.0
65.0
76.5
89.7
19.1
20.3
15.9
13.4
12.7
12.2
4.4
4.0
64.6
64.7
73.2
59.8
3.8
3.0
6.5
22.9
27.6
25.9
14.5
13.4
11.1
10.5
2.3
1.6
59.6
62.0
78.4
77.4
1.8
1.8
4.9
7.7
17.8
20.1
18.5
17.0
7.9
8.4
7.7
7.2
73.2
70.3
72.8
74.7
10.7
9.1
3.9
2.4
5.7
4.2
1.0
0.6
83.4
86.3
94.5
93.3
0.3
0.5
0.7
3.7
26.5
25.8
13.7
5.1
11.7
11.0
8.4
1.7
61.5
62.8
76.1
86.9
0.5
0.6
1.8
6.1
30.9
31.5
29.4
18.4
22.1
20.6
17.4
9.1
45.5
46.3
50.9
69.6
1.7
1.8
2.6
3.0

B

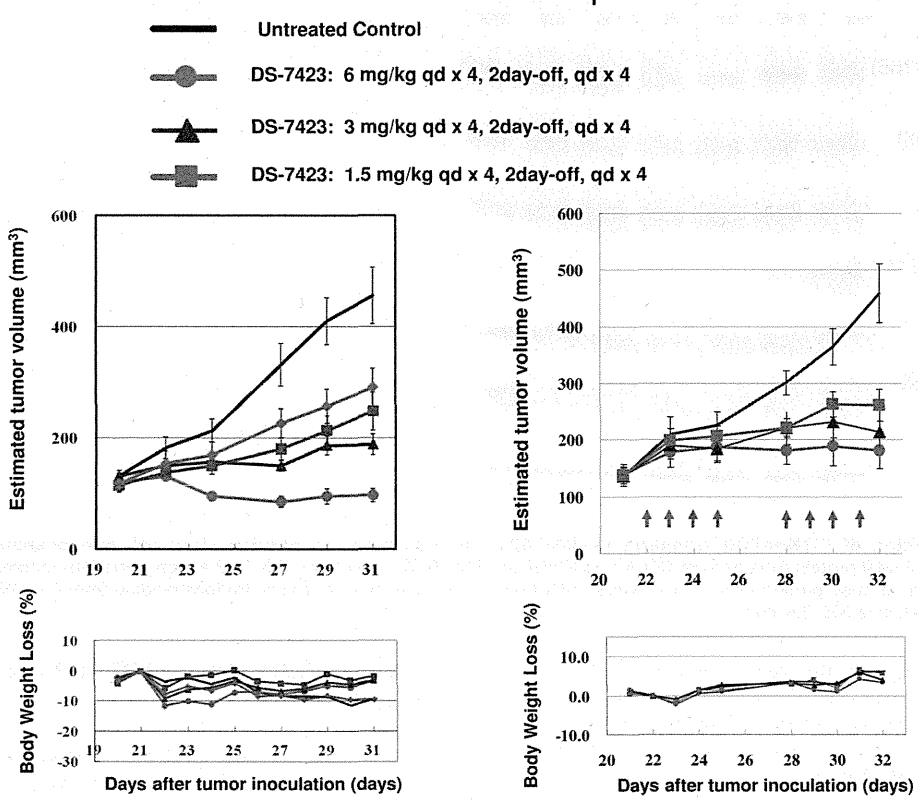
Untreated Control
DS-7423: 6 mg/kg qd x 4, 2day-off, qd x 4
DS-7423: 3 mg/kg qd x 4, 2day-off, qd x 4
DS-7423: 1.5 mg/kg qd x 4, 2day-off, qd x 4
Estimated tumor volume (mm3)
Body Weight Loss (%)
Days after tumor inoculation (days)

Figure 4. Flow cytometric analysis of the cell cycle in cancer cells treated with DS-7423, and *in vivo* demonstration of the anti-tumor effect of DS-7423 in nude mice. (A) Cells (5×10^5) were seeded in the presence of 10% serum and treated with DS-7423 for 48 h at doses of 9.8 nM, 256 nM, or 2,500 nM. DS-7423 blocked OCCA cell cycle progression into the S phase in a dose-dependent manner. The relative size of the sub-G1 population was increased in six of the cell lines (left) but was not affected in the remaining three cell lines (right). (B) Subcutaneous xenograft tumors in athymic BALB/c mice were established following the injection of OCCA cells of either the TOV-21G (left) or RMG-I (right) cell lines. Mice were treated daily (5–7 days per week) at the indicated doses of DS-7423 (1.5, 3, or 6 mg/kg, 8–10 days). Each treatment group contained five mice. Estimated tumor volumes (upper graphs) and body weight losses (BWL) (lower graphs) were shown in the two OCCA cells. Tumor volumes were calculated by the formula {(major axis)*(minor axis)^2/2} mm^3. Groups were compared at the end of treatment. Points, mean; bars, standard deviation (SD); *$p<0.05$.
doi:10.1371/journal.pone.0087220.g004

dose-dependent manner (Figure 4B). No significant adverse effects, including body weight loss of more than 10%, were observed in the mice examined (Figure 4B). Treatment with DS-7423 suppressed the levels of p-AKT (Thr308) and p-S6 (Ser240/244) in the TOV-21G and RMG-I xenografts (Figure S2A). Compared with TOV-21G and RMG-I xenografts, the anti-tumor effect of DS-7423 was weaker in xenografts with ES-2, for which the basal level of p-Akt (Thr-308) was low (Figure S2B).

Induction of apoptosis by DS-7423 in TP53 wild-type cell lines

The data collected from FACS analysis suggested that DS-7423 has a cytotoxic and cytostatic effect in certain OCCA cell lines. We combined the DS-7423 treatment (156 nM or 2,500 nM) with double staining with annexin-V FITC and PI to evaluate the proportion of cells that underwent apoptosis. DS-7423 at 156 nM induced apoptosis at 4–12% in five of the six cell lines that lacked mutations in *TP53* (Figure 5A and 5B). In these five cell lines, 2,500 nM DS-7423 induced apoptosis in 10–16% of the cells. In three cell lines with *TP53* mutations, DS-7423 did not induce apoptosis in >5% of the cells at any of the doses tested (Figure 5A). The size of the population of apoptotic cells was significantly higher in cells that lacked mutations in *TP3* when compared with cells with mutated *TP3* at either 156 nM ($p = 0.0352$) or 2,500 nM ($p = 0.0368$) DS-7423 according to the Student *t*-test (Figure 5C). Rapamycin did not induce apoptotic cell death in >5% of the OCCA cells, even at 2,500 nM. The percentage of apoptotic cells was significantly higher in OVISE cells treated with DS-7423 than that in those treated with rapamycin (Figure S3). This result indicates that mTORC1 inhibition alone is insufficient to induce apoptosis in OCCA cell lines. Immunoblotting analysis revealed that DS-7423 induced the cleavage of PARP within 2 h in OVMANA cells without mutations in *TP53* (Figure 5D). The induction of cleaved-PARP was observed at 39 nM, and the effect increased in a dose-dependent manner up to a concentration of 2,500 nM (Figure 5D).

Induction of p-TP53 at Ser46 and expression of *p53AIP1* by DS-7423

The phosphorylation of MDM2 is associated with the activation of MDM2 and degradation of TP53, with the phosphorylation of TP53 at Ser46 playing a key event in the TP53-dependent apoptosis (28). Treatment with DS-7423 reduced the level of p-MDM2 in a dose-dependent manner (Figure 3A and 6A). Inversely, DS-7423 increased TP53 level even at lower doses, resulting in increased expression of p-TP53 (Ser15 and Ser46) (Figure 6A). However, only p-TP53 (Ser46), not p-TP53 (Ser15), was clearly induced by high doses of DS-7423 (156–2,500 nM). We then used semi-quantitative RT-PCR to evaluate the regulation of genes that are directly regulated by TP53 in OVMANA and OVISE cells. DS-7423 induced the expression of the pro-apoptotic genes *p53AIP1* and *PUMA* at 39 nM or higher doses, but did not induce the expression of p21 at any of the three doses tested (39, 156, and 2,500 nM) (Figure. 6B and 6C). We also performed semi-quantitative RT-PCR of other TP53 target genes involved in DNA repair (p53R2), metabolism (TIGAR and GLS2), G2/M arrest (GADD45), and cell cycle arrest/senescence (14-3-3 sigma and PAI-1) to test whether other TP53 target genes are induced by DS-7423. GADD45 was significantly induced by DS-7423 in OVISE cells (Figure 6B and 6C), in which G2/M arrest was enhanced by DS-7423 according to the MTT assay (Figure 4A). The other TP53-downstream genes tested were not induced by DS-7423 in both OVISE and OVMANA cells, and expression of TIGAR was rather decreased in OVMANA cells (Figure S4).

TP53 activation is responsible for DS-7423-mediated apoptosis

We used siRNAs specific to *TP53* to knockdown *TP53* expression in OVISE cells, and treated the cells with DS-7423 at either 156 or 2,500 nM. The size of the population of apoptotic cells was calculated by annexin-V FITC–PI double staining 48 h after treatment of DS-7423. Knockdown of TP53 levels rescued cells from apoptotic cell death induced by treatment with both DS-7423 doses (Figure 6D). Immunoblotting indicated that two independent siRNAs (siRNA1 and siRNA2) specific to TP53 suppressed the expression of TP53 by >80% (Figure 6E). Next, we performed the MTT assay by applying both DS-7423 and siRNA to TP53 in OVISE cells (wild-type TP53). The anti-proliferative effect of DS-7423 was significantly reduced when combined with the knockdown of TP53 (Figure 6F). The effect of DS-7423 on the transcriptional activity of TP53 was also examined by luciferase assays in ES-2 cells with mutations in *TP53*. The cells were treated with DS-7423 for 24 h at the indicated doses, and then cotransfected with both pp53-TA-luc plasmid (containing TP53 binding sites) and a plasmid that encodes TP53. The relative luciferase activity of TP53 was significantly enhanced by DS-7423 in a dose-dependent manner (Figure 6G).

Discussion

The effects of the PI3K/mTOR inhibitor, DS-7423, on OCCA cell lines were examined with a particular focus on (i) the anti-proliferative effect of DS-7423, (ii) the induction of apoptosis by DS-7423, and (iii) the identification of predictive biomarkers for (i) and (ii).

MTT assays revealed a clear dose-dependent effect of DS-7423 on cell proliferation, with all nine OCCA cell lines displaying sensitivity to DS-7423 (IC_{50} at 75 nM or lower), regardless of mutations on *PIK3CA*. The sensitivity to DS-7423 was significantly higher in OCCA than in OSA cell lines. The prevalence in OCCA cell lines of activating mutations in genes that encode components of the RTK-PI3K-AKT signaling pathway might account, at least in part, for their broad sensitivity to DS-7423. Differences in the dose-dependence of the anti-proliferative effects of DS-7423 and rapamycin suggest differences in the modes of action of these two drugs. Whereas DS-7423 showed a more robust anti-proliferative

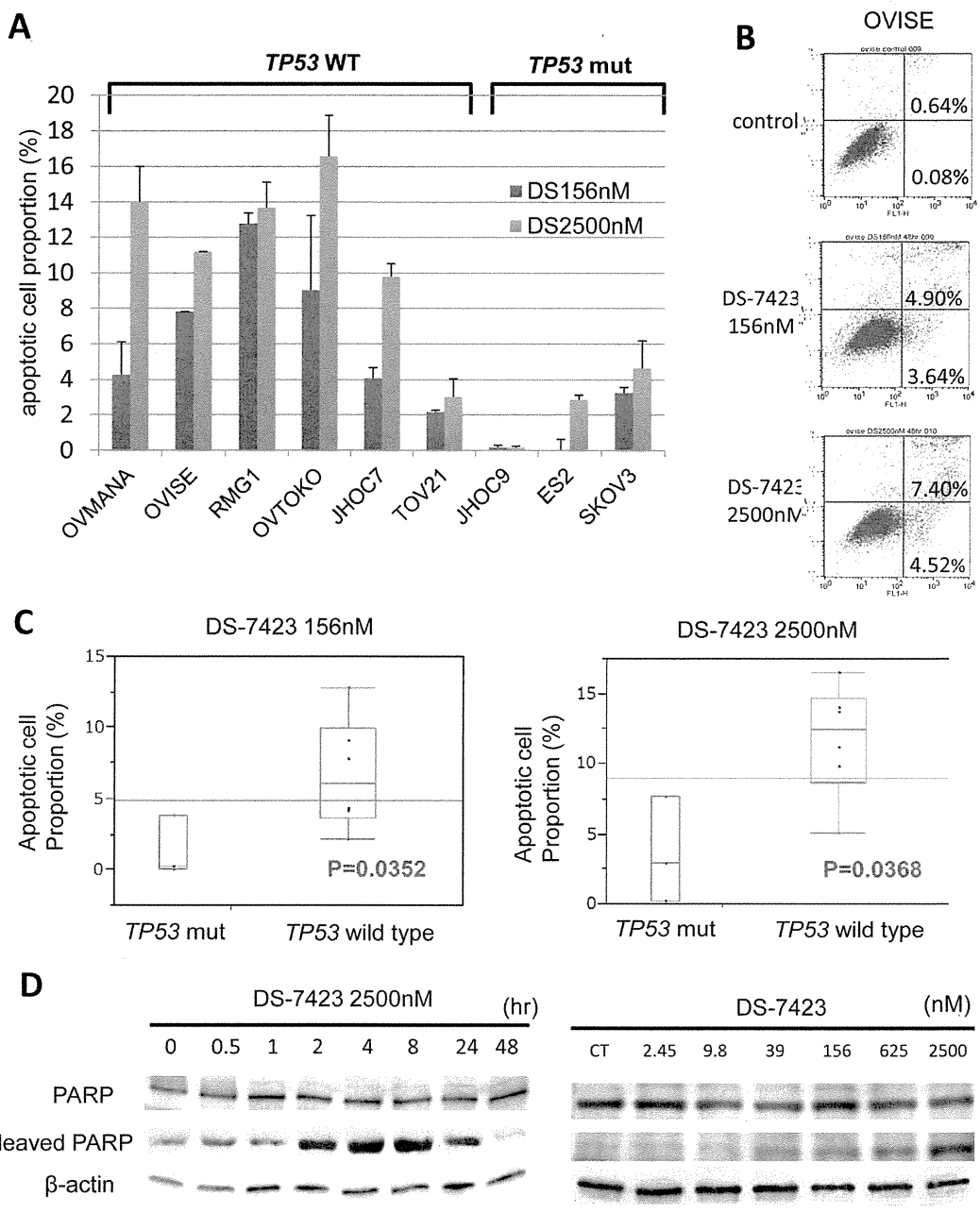

Figure 5. DS-7423–mediated induction of apoptosis in ovarian clear cell adenocarcinoma cell lines. (A) All nine OCCA cells were treated with DS-7423 at 156 or 2,560 nM for 48 h, and apoptotic cell proportion was evaluated using annexin-V fluorescein isothiocyanate (FITC) and propidium iodide (PI) double staining, followed by analysis using flow cytometry. The experiments were repeated 3 times, and each value is shown as the mean of 3 experiments ± standard deviation (SD). (B) The apoptotic cells were calculated using flow cytometry by counting the cell population in the right boxes. The example shown (OVISE cells) is representative of the results obtained for all the cell lines tested. (C) The proportion of cells rendered apoptotic by exposure to DS-7423 at 156 nM and 2,560 nM was significantly higher in OCCA cells without mutations in TP53 than in OCCA cells that carry mutations in TP53. (D) Cleaved poly(ADP-ribose) polymerase (PARP) induction was evaluated by immunoblotting in OVISE cells. OVISE cells were treated with DS-7423 at 156 nM for the times indicated (left) or for 4 h at the doses indicated (right).
doi:10.1371/journal.pone.0087220.g005

effect at the higher concentrations tested (>40 nM), rapamycin suppressed cell proliferation even at lower concentrations (<10 nM), and concentrations >10 nM failed to suppress the proliferation any further. This dose dependency is compatible with the phosphorylation levels of the target proteins in immunoblotting data and several previous reports in other types of cancers [10,12,36]. The cell cycle profile was distinct among each cell line. For example, G1 arrest was not induced and G2/M ratio was high in OVISE cells under DS-7423 exposure. This might be partly explained by the fact that GADD45 was induced by DS-7423 in

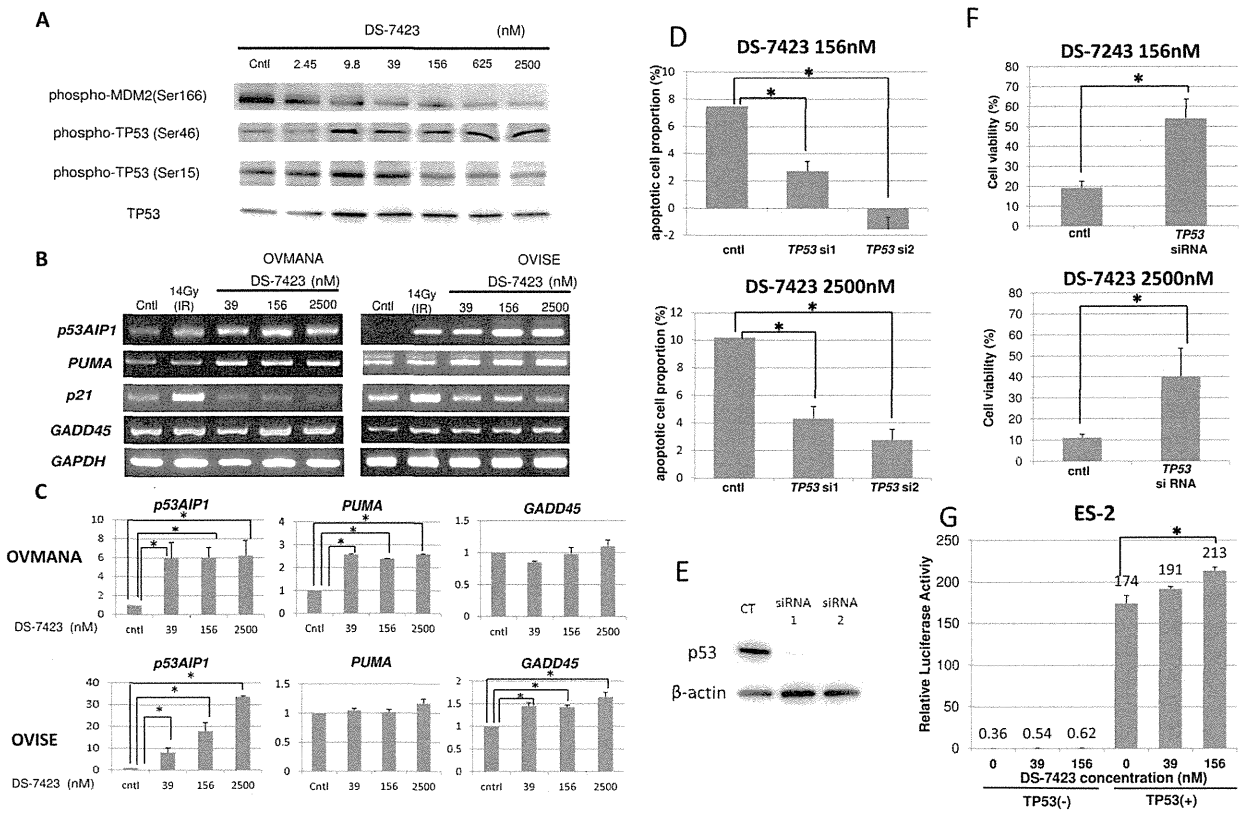

Figure 6. Induction of the phosphorylation of TP53 at Ser46 and the accumulation of transcripts of the genes targeted by TP53, which participate in TP53-mediated apoptosis. (A) Immunoblotting in OVMANA cells treated with DS-7423 at the indicated doses. Phosphorylation levels of MDM2 were inversely associated with p-TP53 at Ser46, but not with p-TP53 at Ser15. (B) Semi-quantitative RT-PCR in OVMANA and OVISE cells treated with DS-7423 at the indicated doses. Both *p53AIP1* and *PUMA* were induced by DS-7423. CT, untreated (negative) control; IR, irradiation at 14 Gy (positive control). GADD45 was induced in OVISE, but not in OVMANA cells. (C) Quantification of the semi-quantitative RT-PCR in (B). Each experiment was repeated 3 times, and each value is shown as the mean of 3 experiments ± SD. *$p<0.05$ (D) Effect of *TP53* knockdown on apoptosis induction by DS-7423. TP53 was knocked down by two independent siRNAs specific to *TP53* (siRNA1 and 2) in OVISE cells, which do not carry any mutation in *TP53*. The apoptotic cell population was evaluated using annexin-V staining, as described in Figure 5. The experiments were repeated 3 times, and each value is shown as the mean of 3 experiments ± SD. *$p<0.05$ (E) Suppression of TP53 expression by siRNAs was confirmed by immunoblotting. (F) Effect of *TP53* knockdown on cell proliferation by DS-7423 in MTT assay of OVISE cells. TP53 was knocked down by a siRNA1 specific to *TP53* and MTT assay was subsequently performed as in Figure 2. Knockdown of TP53 diminished the anti-proliferative effect caused by DS-7423 on OVISE cells. The experiments were repeated 3 times, and each value is shown as the mean of 3 experiments ± SD. *$p<0.05$ (G) TP53 expression plasmid (0.1 μg/μL) was cotransfected with pp53 TA Luc (0.25 μg/mL) plasmid into ES-2 cells mutated in *TP53*. The addition of DS-7423 increased the relative luciferase activity of TP53 in a dose-dependent manner. The experiments were repeated 3 times, and each value is shown as the mean of 3 experiments ± SD. *$p<0.05$.

doi:10.1371/journal.pone.0087220.g006

these cells. Thus, the action mechanism of DS-7423 might be distinct in each type of cells, regardless of the TP53 status. Resistance to mTOR (mTORC1) inhibitors might be induced by several mechanisms, including increased activity of another mTOR complex, mTORC2, or upregulation of receptor tyrosine kinases such as insulin-like growth factor-1 receptor (IGF-R1) [37,38]. The use of mTORC1 inhibitors to treat OCCAs is currently being investigated in phase 2 clinical trials. The currently ongoing GOG (Gynecologic Oncology Group)-0268 (NCT01196429) trial recruits OCCA patients and treats the subjects with carboplatin and paclitaxel, followed by temsirolimus (CCI-779). A report on six cases with weekly administration of temsirolimus in recurrent OCCA patients showed partial response in one patient and stable disease in another patient [39]. However, given that our data suggest that dual PI3K/mTOR inhibitors, such as DS-7423, might be more promising than single mTORC1 inhibitors, clinical trials that involve a dual PI3K/mTOR inhibitor, such as DS-7423, seem warranted for OCCA.

DS-7423 induced significantly higher levels of apoptotic cell death in OCCA cells without mutations in *TP53* than in OCCA cells with *TP53* mutations. This result suggests both that the mutational status of *TP53* might be a good biomarker to predict apoptosis induction by DS-7423, and that apoptosis depends on TP53 function. TP53 is degraded by MDM2, a ubiquitin ligase for TP53, and the MDM2 function is augmented by the kinase activity of Akt. Akt-mediated phosphorylation of MDM2 blocks its binding to p19ARF, increasing the degradation of TP53 [40,41]. DS-7423 increased the level of p-TP53 at Ser46, which results in induction of *p53AIP1* and *PUMA* (genes involved in TP53-mediated apoptosis) [29,42–44]. This data suggests that the apoptotic effect of DS-7423 depends, at least in part, on TP53 activity. The reasons for p-TP53 (Ser46), not p-TP53 (Ser15), being clearly induced and for apoptosis being preferentially

induced by high doses of DS-7423 should be further clarified. In addition, other non-apoptotic genes were not significantly induced by DS-7423, except for GADD45 in OVISE cells. Further analyses are warranted whether TP53 function is more involved in apoptosis rather than in cell cycle arrest and/or DNA repair process by DS-7423. Another possibility is that other proteins (such as FOXOs) which act downstream of Akt might also play a role in the induction [45]. Dephosphorylation of FOXOs at their Akt sites induces their nuclear translocation and triggers apoptosis by induction of prosurvival genes of the BCL2 family [46,47]. The observation that the phosphorylation of FOXO1/3a was suppressed by DS-7423, regardless of TP53 status, suggests that the pro-apoptotic effect of DS-7423 cannot be explained exclusively by the phosphorylation of FOXOs. The use of siRNA to knockdown TP53 rescued OCCA cells from apoptosis caused by DS-7423. We also confirmed by MTT assay that the anti-proliferative effect of DS-7423 was significantly diminished by knocking down TP53, suggesting that intact TP53 function might enhance the anti-tumor effect of DS-7423. Recently, it was reported that cell death caused by a PI3K inhibitor, BKM-120, was associated with TP53 status in glioma cells [48], and that PI3K/AKT inhibition was suggested to induce TP53-dependent apoptosis in HTLV-1-transformed cells [49]. These data also support the importance of wild-type TP53 in the induction of the cytotoxic effect of PI3K pathway inhibitors.

The involvement of multiple molecules in the activation of the PI3K/mTOR pathway underscores the critical need to develop predictive biomarkers that might also serve as therapeutic targets. Mutations of *PIK3CA* and amplification of *HER2* have been proposed to be useful biomarkers in breast cancer [50,51], whereas mutant Ras has been suggested to be a biomarker of resistance in several solid tumor cells [52]. All these biomarkers (*PIK3CA*, HER2 and Ras) are focused on the RTK/Ras/PI3K pathway itself, and not on the cytotoxic effects associated with PI3K/mTOR inhibitors. Our data suggest that the presence of *PIK3CA* mutation and any other PI3K-activating alteration alone might not predict the sensitivity of OCCA cells to DS-7423. ES-2 cells, with no mutations in the RTK/Ras/PI3K pathway genes examined, showed low level of p-Akt, and the effect of DS-7423 in ES-2 xenografts was less robust, suggesting that the level of PI3K pathway activation would still be important for the sensitivity. However, the mutational status of TP53 might represent a better biomarker for the selection of tumors that could be killed by DS-7423 treatment. The frequency of mutations in *TP53* in OCCA was much less frequent than for ovarian cancers with other histology types [15,53]. These results indicate that OCCAs would be good candidates for clinical studies on the dual PI3K/mTOR inhibitor, DS-7423.

Our study has several limitations. First, cytostatic effect is still essential to suppress cell proliferation, regardless of TP53 status. Second, the ratio of apoptotic cells is low (less than 20%) even at high concentrations of DS-7423. Third, the mechanism of cytostatic effect by DS-7423 in OCCA is cell type dependent (i.e. G1 arrest was not induced in OVISE and ES-2 cells). Thus, careful consideration is required to evaluate the TP53-dependent cytotoxic effect of DS-7423. Further studies are warranted to elucidate the mechanism of action of DS-7423, and more efficient induction of apoptosis might be needed for clinical application of this drug in OCCA.

Supporting Information

Figure S1 Immunoblotting of OCCA cells (ES-2 and JHOC-9), treated with DS-7423 at concentrations ranging from 0 to 2,500 nmol/L. As shown in Figure 3, phosphorylation of AKT and its target proteins were downregulated by DS-7423. In ES-2 cells, basal level of p-AKT at Thr 308 was very low (as shown in Fig. 1), but p-AKT at Ser473 was clearly suppressed by DS-7423.
(PPTX)

Figure S2 *In vivo* effect of DS-7423 in nude mice. (A) Western blot of total lysates from the TOV-21G and RMG-1 xenografts. total lysates were harvested 2 and 6 h after the last drug administration of DS-7423. The levels of p-Akt (Thr-308) and p-S6 (Ser-240/244) were assessed. (B) Subcutaneous xenograft tumors in athymic BALB/c mice were established after injection of ES-2 cells. Mice were treated daily at the indicated doses (1.5, 3 or 6 mg/kg/day, totally 8 times) of DS-7423 or non-treated control. Estimated tumor volumes were smaller in mice treated daily with 6 mg/kg of DS-7423, compared to the control. Western blot of total lysates from the ES-2 xenografts (treated with 6 mg/kg of DS-7423) was also shown below.
(PPTX)

Figure S3 The size of apoptotic cell population was compared between DS-7423 and rapamycin in OVISE cells, using annexin-V FITC and PI double staining (as shown in Fig. 5A–5B). The percentage of apoptotic cells was significantly higher in cells treated with DS-7423, compared with those with rapamycin.
(PPTX)

Figure S4 Semi-quantitative RT-PCR in OVMANA and OVISE cells treated with DS-7423 at the indicated doses. Each expression level of p53R2, TIGAR, GLS2, GADD45, 14-3-3 sigma and PAI-1 was not enhanced by DS-7423. Each experiment was repeated 3 times, and each value is shown as the mean of 3 experiments ± SD.
(PPTX)

Table S1 Phosphorylation and mutational status in 9 OCCA cell lines. Elevated phosphorylation of cMET, HER2 and HER3, and mutations of *PIK3CA*, *PTEN*, *KRAS* and *TP53* were listed in each cell line.
(XLSX)

Acknowledgments

We thank Satoru Kyo for the generous gift of the immortalized cell line.

Author Contributions

Conceived and designed the experiments: T Kashiyama KO YS YH KM. Performed the experiments: T Kashiyama YI YS YH KI CM RK. Analyzed the data: T Kashiyama KO YS YH. Contributed reagents/materials/analysis tools: YI AM T Koso T Fukuda MT K Shoji K Sone TA OW-H KK SN KM FM HA TY YO T Fujii. Wrote the paper: T Kashiyama KO.

References

1. Yuan TL, Cantley LC (2008) PI3K pathway alterations in cancer: variations on a theme. Oncogene 27: 5497–510.
2. Jia S, Liu Z, Zhang S, Liu P, Zhang L, et al. (2008) Essential roles of PI(3)K-p110beta in cell growth, metabolism and tumorigenesis. Nature 454: 776–9.
3. Wee S, Wiederschain D, Maira SM, Loo A, Miller C, et al. (2008) PTEN-deficient cancers depend on PIK3CB. Proc Natl Acad Sci USA 105: 13057–13062.
4. Zoncu R, Efeyan A, Sabatini DM (2011) mTOR: from growth signal integration to cancer, diabetes and ageing. Nat Rev Mol Cell Biol 12: 21–35.

5. Engelman JA (2009) Targeting PI3K signalling in cancer: opportunities, challenges and limitations. Nat Rev Cancer 9: 550–562.
6. Sabatini DM (2006) mTOR and cancer: insights into a complex relationship. Nat Rev Cancer 6: 729–734.
7. Guertin DA, Sabatini DM (2007) Defining the role of mTOR in cancer. Cancer Cell 12: 9–22.
8. Mayo LD, Donner DB (2001) A phosphatidylinositol 3-kinase/Akt pathway promotes translocation of Mdm2 from the cytoplasm to the nucleus. Proc Natl Acad Sci USA 98: 11598–11603.
9. Maira SM, Stauffer F, Brueggen J, Furet P, Schnell C, et al. (2008) Identification and characterization of NVP-BEZ235, a new orally available dual phosphatidylinositol 3-kinase/mammalian target of rapamycin inhibitor with potent in vivo antitumor activity. Mol Cancer Ther 7: 1851–1863.
10. Serra V, Markman B, Scaltriti M, Eichhorn PJ, Valero V, et al. (2008) NVP-BEZ235, a dual PI3K/mTOR inhibitor, prevents PI3K signaling and inhibits the growth of cancer cells with activating PI3K mutations. Cancer Res 68: 8022–8030.
11. Cao P, Maira SM, Garcia Echeverria C, Hedley DW (2009) Activity of a novel, dual PI3-kinase/mTor inhibitor NVP-BEZ235 against primary human pancreatic cancers grown as orthotopic xenografts. Br J Cancer 100: 1267–1276.
12. Shoji K, Oda K, Kashiyama T, Ikeda Y, Nakagawa S, et al. (2012) Genotype-dependent efficacy of a dual PI3K/mTOR inhibitor, NVP-BEZ235, and an mTOR inhibitor, RAD001, in endometrial carcinomas. PLoS One 7: e37431.
13. Anglesio MS, Carey MS, Kobel M, Mackay H, Huntsman DG (2011) Clear cell carcinoma of the ovary: A report from the first Ovarian Clear Cell Symposium, June 24th, Gynecol Oncol 2010. 121: 407–415.
14. Takano M, Tsuda H, Sugiyama T (2012) Clear cell carcinoma of the ovary: is there a role of histology-specific treatment? J Exp Clin Cancer Res 31: 53–59.
15. Bell D, Berchuck A, Birrer M, Chien J, Cramer D, et al. (2011) Integrated genomic analyses of ovarian carcinoma. Nature 474: 609–615. Cancer Genome Atlas Research Network.
16. Ho ES, Lai CR, Hsieh YT, Chen JT, Lin AJ, et al. (2001) p53 mutation is infrequent in clear cell carcinoma of the ovary. Gynecol Oncol 80: 189–193.
17. Kuo KT, Mao TL, Jones S, Veras E, Ayhan A, et al. (2009) Frequent activating mutations of PIK3CA in ovarian clear cell carcinoma. Am J Pathol 174: 1597–1601.
18. Munksgaard PS, Blaakaer J (2012) The association between endometriosis and ovarian cancer: a review of histological, genetic and molecular alterations. Gynecol Oncol 124: 164–169.
19. Fujimura M, Katsumata N, Tsuda H, Uchi N, Miyazaki S, et al. (2002) HER2 is frequently over-expressed in ovarian clear cell adenocarcinoma: possible novel treatment modality using recombinant monoclonal antibody against HER2, trastuzumab. Jpn J Cancer Res 93: 1250–1257.
20. Yamamoto S, Tsuda H, Miyai K, Takano M, Tamai S, et al. (2011) Gene amplification and protein overexpression of MET are common events in ovarian clear-cell adenocarcinoma: their roles in tumor progression and prognostication of the patient. Mod Pathol 24: 1146–1155.
21. Yamamoto S, Tsuda H, Miyai K, Takano M, Tamai S, et al. (2012) Accumulative copy number increase of MET drives tumor development and histological progression in a subset of ovarian clear-cell adenocarcinomas. Mod Pathol 25: 122–130.
22. Shaw TJ, Senterman MK, Dawson K, Crane CA, Vanderhyden BC (2004) Characterization of intraperitoneal, orthotopic, and metastatic xenograft models of human ovarian cancer. Mol Ther 10: 1032–1042.
23. Bono Y, Kyo S, Takakura M, Maida Y, Mizumoto Y, et al. (2012) Creation of immortalised epithelial cells from ovarian endometrioma. Br J Cancer 106: 1205–1213.
24. Minaguchi T, Yoshikawa H, Oda K, Ishino T, Yasugi T, et al. (2001) PTEN mutation located only outside exons 5, 6, and 7 is an independent predictor of favorable survival in endometrial carcinomas. Clin Cancer Res 7: 2636–2642.
25. Samuels Y, Wang Z, Bardelli A, Silliman N, Ptak J, et al. (2004) High frequency of mutations of the PIK3CA gene in human cancers. Science 304: 554.
26. Oda K, Stokoe D, Taketani Y, McCormick F (2005) High frequency of coexistent mutations of PIK3CA and PTEN genes in endometrial carcinoma. Cancer Res 65: 10669–10673.
27. Oda K, Okada J, Timmerman L, Rodriguez Viciana P, Stokoe D, et al. (2008) PIK3CA cooperates with other phosphatidylinositol 3′-kinase pathway mutations to effect oncogenic transformation. Cancer Res 68: 8127–8136.
28. Nakagawa S, Yoshikawa H, Jimbo H, Onda T, Yasugi T, et al. (1999) Elderly Japanese women with cervical carcinoma show higher proportions of both intermediate-risk human papillomavirus types and p53 mutations. Br J Cancer 79: 1139–1144.
29. Oda K, Arakawa H, Tanaka T, Matsuda K, Tanikawa C, et al. (2000) p53AIP1, a potential mediator of p53-dependent apoptosis, and its regulation by Ser-46-phosphorylated p53. Cell 102: 849–862.
30. Hermeking H, Lengauer C, Polyak K, He TC, Zhang L, et al (1997) 14-3-3 sigma is a p53-regulated inhibitor of G2/M progression. Mol Cell 1: 3–11.
31. Zhan Q, Antinore MJ, Wang XW, Carrier F, Smith ML, et al (1999) Association with Cdc2 and inhibition of Cdc2/Cyclin B1 kinase activity by the p53-regulated protein Gadd45. Oncogene 18: 2892–2900.
32. Tanaka H, Arakawa H, Yamaguchi T, Shiraishi K, Fukuda S, et al (2000) A ribonucleotide reductase gene involved in a p53-dependent cell-cycle checkpoint for DNA damage. Nature 404: 42–49.
33. Kortlever RM, Higgins PJ, Bernards R (2006) Plasminogen activator inhibitor-1 is a critical downstream target of p53 in the induction of replicative senescence. Nat Cell Biol 8: 877–884.
34. Bensaad K, Tsuruta A, Selak MA, Vidal MN, Nakano K, et al (2006) TIGAR, a p53-inducible regulator of glycolysis and apoptosis. Cell 126: 107–120.
35. Suzuki S, Tanaka T, Poyurovsky MV, Nagano H, Mayama T, et al (2010) Phosphate-activated glutaminase (GLS2), a p53-inducible regulator of glutamine metabolism and reactive oxygen species. Proc Natl Acad Sci U S A 107: 7461–7466.
36. Cho DC, Cohen MB, Panka DJ, Collins M, Ghebremichael M, et al. (2010) The efficacy of the novel dual PI3-kinase/mTOR inhibitor NVP-BEZ235 compared with rapamycin in renal cell carcinoma. Clin Cancer Res 16: 3628–3638.
37. O'Reilly KE, Rojo F, She QB, Solit D, Mills GB, et al. (2006) mTOR inhibition induces upstream receptor tyrosine kinase signaling and activates Akt. Cancer Res 66: 1500–1508.
38. Wan X, Harkavy B, Shen N, Grohar P, Helman LJ (2007) Rapamycin induces feedback activation of Akt signaling through an IGF-1R-dependent mechanism. Oncogene 26: 1932–1940.
39. Takano M, Kikuchi Y, Kudoh K, Goto T, Furuya K, et al. (2011) Weekly administration of temsirolimus for heavily pretreated patients with clear cell carcinoma of the ovary: a report of six cases. Int J Clin Oncol 16: 605–609.
40. Haupt Y, Maya R, Kazaz A, Oren M (1997) Mdm2 promotes the rapid degradation of p53. Nature 387: 296–299.
41. Ogawara Y, Kishishita S, Obata T, Isazawa Y, Suzuki T, et al. (2002) Akt enhances Mdm2-mediated ubiquitination and degradation of p53. J Biol Chem 277: 21843–21850.
42. Nakano K, Vousden KH (2001) PUMA, a novel proapoptotic gene, is induced by p53. Mol Cell 7: 683–694.
43. Matsuda K, Yoshida K, Taya Y, Nakamura K, Nakamura Y, et al. (2002) p53AIP1 regulates the mitochondrial apoptotic pathway. Cancer Res 62: 2883–2889.
44. Vousden KH, Prives C (2009) Blinded by the Light: The Growing Complexity of p53. Cell 137: 413–421.
45. Fu Z, Tindall DJ (2008) FOXOs, cancer and regulation of apoptosis. Oncogene 27: 2312–2319.
46. Rahmani M, Anderson A, Habibi JR, Crabtree TR, Mayo M, et al. (2009) The BH3-only protein Bim plays a critical role in leukemia cell death triggered by concomitant inhibition of the PI3K/Akt and MEK/ERK1/2 pathways. Blood 114: 4507–4516.
47. Letai A (2006) Growth factor withdrawal and apoptosis: the middle game. Mol Cell 21: 728–730.
48. Koul D, Fu J, Shen R, LaFortune TA, Wang S, et al (2012) Antitumor activity of NVP-BKM120– a selective pan class I PI3 kinase inhibitor showed differential forms of cell death based on p53 status of glioma cells. Clin Cancer Res 18: 184–195.
49. Jeong SJ, Dasgupta A, Jung KJ, Um JH, Burke A, et al (2008) PI3K/AKT inhibition induces caspase-dependent apoptosis in HTLV-1-transformed cells. Virology 370: 264–272.
50. She QB, Chandarlapaty S, Ye Q, Lobo J, Haskell KM, et al. (2008) Breast tumor cells with PI3K mutation or HER2 amplification are selectively addicted to Akt signaling. PLoS One 3: e3065.
51. O'Brien C, Wallin JJ, Sampath D, GuhaThakurta D, Savage H, et al. (2010) Predictive biomarkers of sensitivity to the phosphatidylinositol 3′ kinase inhibitor GDC-0941 in breast cancer preclinical models. Clin Cancer Res 16: 3670–3683.
52. Ihle NT, Lemos R Jr, Wipf P, Yacoub A, Mitchell C, et al. (2009) Mutations in the phosphatidylinositol-3-kinase pathway predict for antitumor activity of the inhibitor PX-866 whereas oncogenic Ras is a dominant predictor for resistance. Cancer Res 69: 143–150.
53. Petitjean A, Achatz MI, Borresen Dale AL, Hainaut P, et al. (2005) TP53 mutations in human cancers: functional selection and impact on cancer prognosis and outcomes. Oncogene 26: 2157–2165.

Research Article

EASL EUROPEAN ASSOCIATION FOR THE STUDY OF THE LIVER | JOURNAL OF HEPATOLOGY

The AMPK-related kinase SNARK regulates hepatitis C virus replication and pathogenesis through enhancement of TGF-β signaling

Kaku Goto[1,2,3], Wenyu Lin[1], Leiliang Zhang[1], Nikolaus Jilg[1], Run-Xuan Shao[1], Esperance A.K. Schaefer[1], Hong Zhao[1], Dahlene N. Fusco[1], Lee F. Peng[1], Naoya Kato[2], Raymond T. Chung[1,*]

[1]*Gastrointestinal Unit, Department of Medicine, Massachusetts General Hospital, Harvard Medical School, Boston, MA 02114, USA;*
[2]*The Advanced Clinical Research Center, The Institute of Medical Science, The University of Tokyo, Tokyo 108-8639, Japan;*
[3]*Japan Society for the Promotion of Science, Tokyo 102-8472, Japan*

Background & Aims: Hepatitis C virus (HCV) is a major cause of chronic liver disease worldwide. The biological and therapeutic importance of host cellular cofactors for viral replication has been recently appreciated. Here we examined the roles of SNF1/AMP kinase-related kinase (SNARK) in HCV replication and pathogenesis.
Methods: The JFH1 infection system and the full-length HCV replicon OR6 cell line were used. Gene expression was knocked down by siRNAs. SNARK mutants were created by site-directed mutagenesis. Intracellular mRNA levels were measured by qRT-PCR. Endogenous and overexpressed proteins were detected by Western blot analysis and immunofluorescence. Transforming growth factor (TGF)-β signaling was monitored by a luciferase reporter construct. Liver biopsy samples from HCV-infected patients were analyzed for SNARK expression.
Results: Knockdown of SNARK impaired viral replication, which was rescued by wild type SNARK but not by unphosphorylated or kinase-deficient mutants. Knockdown and overexpression studies demonstrated that SNARK promoted TGF-β signaling in a manner dependent on both its phosphorylation and kinase activity. In turn, chronic HCV replication upregulated the expression of SNARK in patients. Further, the SNARK kinase inhibitor metformin suppressed both HCV replication and SNARK-mediated enhancement of TGF-β signaling.
Conclusions: Thus reciprocal regulation between HCV and SNARK promotes TGF-β signaling, a major driver of hepatic fibrogenesis. These findings suggest that SNARK will be an attractive target for the design of novel host-directed antiviral and antifibrotic drugs.

Keywords: SNARK; NUAK2; HCV; Metformin; Fibrosis; TGF-beta; SMAD; Kinase.
Received 5 December 2012; received in revised form 3 June 2013; accepted 19 June 2013; available online 2 July 2013
* Corresponding author. Address: Gastrointestinal Unit, Massachusetts General Hospital, Boston, MA 02114, USA. Tel.: +1 617 724 7562; fax: +1 617 643 0446.
E-mail address: rtchung@partners.org (R.T. Chung).
Abbreviations: SNARK, sucrose-non-fermenting protein kinase 1/AMP-activated protein kinase-related protein kinase; TGF-β, transforming growth factor beta; JFH1, Japanese fulminant hepatitis 1; HTAs, host-targeting antivirals; HCC, hepatocellular carcinoma; SVR, sustained virological response; CsA, cyclosporin A.

Introduction

Chronic infection with hepatitis C virus (HCV) is a major cause of chronic liver disease and hepatocellular carcinoma (HCC) and the leading reason for liver transplantation worldwide. HCV infects approximately 170 million individuals worldwide [1]. Current therapy with pegylated interferon (IFN)-α in combination with ribavirin produces sustained virological response (SVR) in fewer than half of the patients infected with genotype 1 HCV, and does so with high rates of often unacceptable side effects [2]. In recent years, it has become increasingly evident that HCV propagation is highly dependent on host cellular cofactors which in turn represent promising antiviral targets [3]. It is hoped that these strategies will lead to rational host-targeting antivirals (HTAs) [4]. Moreover, HCV interferes with host cellular signaling pathways causing pathogenic effects such as insulin resistance (IR), diabetes, and alterations in host lipids. Indeed, mounting evidence supports hepatitis C as a metabolic disorder [5]. Hence, intervention against key host cellular factors critical for both HCV replication and viral pathogenesis may yield anti-hepatitis C therapies that both halt replication and abrogate other pathogenic effects of HCV, which might be further thought of as host-directed antiviral and antipathogenic therapies. Based on this assumption, we have previously conducted a functional genomic screen for host cellular factors supporting HCV replication using an HCV replicon system [6]. Among positive hits in our original screen was sucrose-non-fermenting protein kinase 1 (SNF1)/AMP-activated protein kinase (AMPK)-related protein kinase (SNARK), the fourth member of 14 mammalian AMPK-related kinases [7], which has been consistently found in other screens [8,9]. Although SNARK function is not well understood, SNARK heterozygote knockout mice displayed elevated serum triglyceride concentrations, hyperinsulinemia, glucose intolerance [10], and impaired contraction-stimulated glucose transport [11], implying that SNARK operates to maintain glucose and lipid homeostasis in a

manner analogous to AMPK, which was recently described to inhibit HCV replication [12].

Transforming growth factor (TGF)-β is a pleiotropic cytokine partaking in cell proliferation, differentiation, apoptosis, migration [13], and the major cytokine responsible for fibrosis in tissues including the liver. In HCV-infected persons, levels of TGF-β are elevated [14], and TGF-β was exhibited to promote the viral replication in a replicon model and was correlated with accelerated liver fibrosis in an *in vivo* model [15,16]. Intriguingly, a prior high-throughput mapping study of protein-protein interaction (PPI) identified an association of SNARK with SMADs [17], implying a direct link of SNARK to TGF-β signaling. Therefore, we sought to examine the significance and potential of SNARK as a therapeutic target in HCV replication and pathogenesis and its contribution to TGF-β signaling. We report that the phosphorylation and phosphotransferase activities of SNARK are required for HCV replication. Furthermore SNARK was demonstrated to enhance TGF-β signaling, and finally chronic HCV infection upregulated the expression of SNARK in patients. SNARK has pleiotropic functions including pro-TGF-β signaling activities in addition to the previously described AMPK-like properties. The finding of a reciprocal regulation between HCV and SNARK suggests that SNARK could be an effective host cellular target not only for an antiviral but also antipathogenic strategy.

Materials and methods

Compounds, antibodies, cells, and viruses

Metformin, TGF-β, and CsA were purchased from EMD chemicals USA (Gibbstown, NJ), Fitzgerald (North Acton, MA), and Sigma-Aldrich (St. Louis, MO), respectively. Antibodies to SNARK, FLAG, and β-actin were obtained from Sigma-Aldrich, and antibodies to HCV NS5A and phosphothreonine were obtained from BioFront Technologies (Tallahassee, FL) and Cell Signaling Technology (Danvers, MA), respectively. HuH7.5.1 and OR6 replicon cells were cultured as described previously [18], and HeLa cells were cultured in DMEM with 10% FBS. JFH1 virus infection was performed as described previously [19].

Further Materials and methods are described in the Supplementary Material section.

Results

Functional SNARK enhances HCV replication

To assess the contribution of SNARK to HCV replication, we first knocked down endogenous SNARK expression (Supplementary Fig. 1) with siRNAs in the Japanese fulminant hepatitis 1 (JFH1) virus infection system. HuH7.5.1 cells were transfected with SNARK-targeted siRNAs, which was followed by JFH1 infection. Reduced levels of *SNARK* mRNA were associated with impaired viral replication (Fig. 1A). We then constructed plasmids encoding the siRNA-resistant *SNARK* open reading frame (ORF) bearing synonymous mutations that are not recognized by *SNARK* siRNAs. The over expression of these siRNA-resistant SNARK proteins successfully rescued *SNARK* RNAi-impaired HCV replication (Fig. 1A, rSN-1 and rSN-7). We also tested the effects of SNARK knockdown and overexpression in the genotype 1 OR6 replicon system, and found that the decreased level of HCV RNA replication was also rescued by overexpression of siRNA-resistant forms of SNARK (Fig. 1B). Thus, SNARK was demonstrated to specifically support HCV replication in both a *bona fide* infection system and replicon model.

Next we sought to identify the function(s) responsible for SNARK's contribution to HCV replication. We introduced single

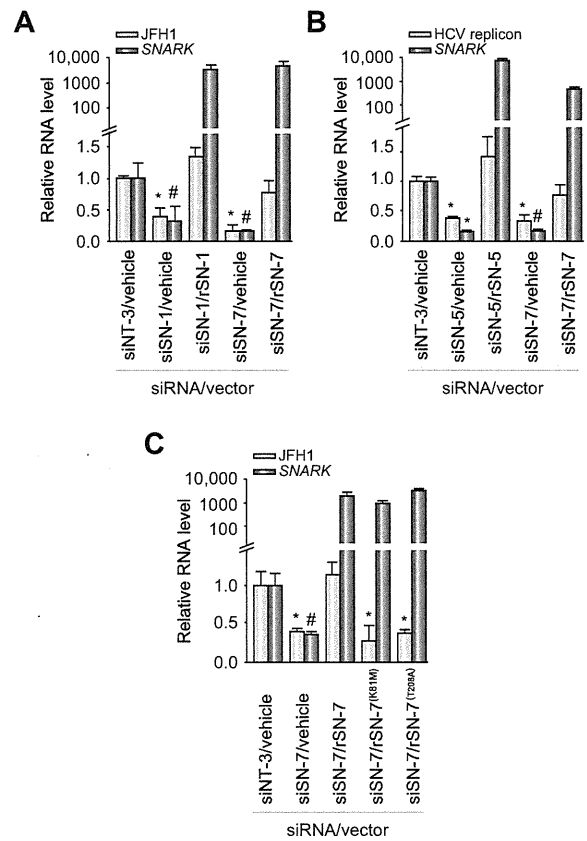

Fig. 1. SNARK supports HCV replication. (A) HuH7.5.1 cells were transfected with either non-targeting (siNT-3) or *SNARK*-targeted siRNAs (siSN-1 and siSN-7), followed by transfection of either empty or siRNA-resistant SNARK expression vectors (rSN-1 and rSN-7) 48 h later. The cells were infected with JFH1 on the next day and total RNA was harvested 48 h later. Relative JFH1 RNA and *SNARK* mRNA levels were quantified by real-time PCR analysis and normalized to *GAPDH*; $^{*}p$ <0.05 or $^{\#}p$ <0.01 *vs.* siNT-3 empty control. (B) OR6 replicon cells were transfected with siRNAs, followed by the transfection of empty or siRNA-resistant SNARK expression vectors 48 h later. Then total RNA was harvested 72 h later. Relative replicon RNA and *SNARK* mRNA levels were quantified by real-time PCR analysis and normalized to *GAPDH*. $^{*}p$ <0.01 or $^{\#}p$ <0.05 *vs.* siNT-3 empty control. (C) The rescue assay was conducted as described in (A). Here expression vectors of siRNA-resistant SNARK with either kinase-deficient mutation (rSN-7 K81M) or phosphorylation-deficient mutation (rSN-7 T208A) were used. Relative JFH1 RNA and *SNARK* mRNA levels were quantified by real-time PCR and normalized to *GAPDH*. $^{*}p$ <0.01 or $^{\#}p$ <0.05 *vs.* siNT-3 empty control.

mutations that abrogate either its phosphotransferase activity in the enzymatic pocket (K81M) or its phosphorylation at the phosphoacceptor site (T208A) in the siRNA-resistant *SNARK* ORF and overexpressed them in the rescue assay system used above with JFH1. In contrast to the rescue effects by wild type SNARK on viral replication, both functionally deficient mutants failed to recover impaired HCV replication by SNARK depletion (Fig. 1C and Supplementary Fig. 2). This result suggested that both the phosphorylation and kinase activities of SNARK are essential for its support of HCV replication.

SNARK phosphotransferase activity can be targeted

In a human hepatocarcinoma cell line, the kinase activity of SNARK was previously reported to be inhibited by metformin

Research Article

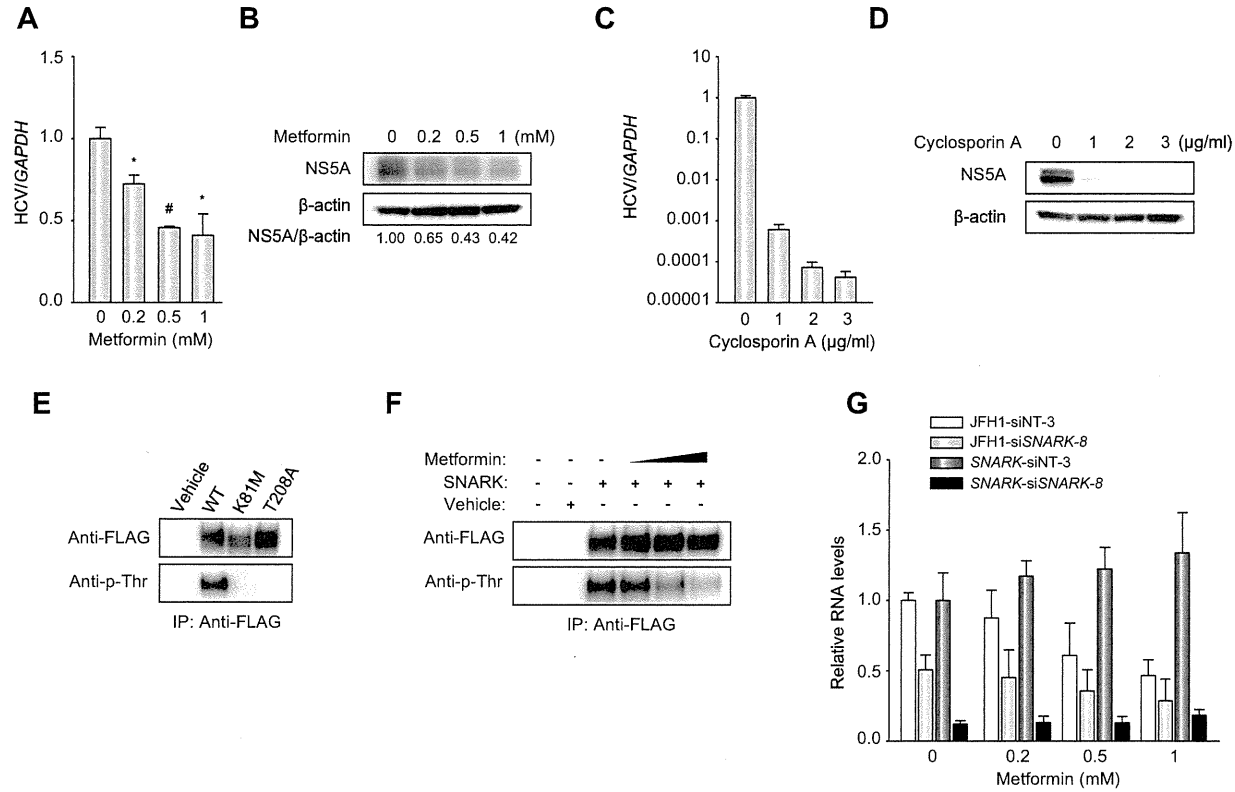

Fig. 2. Metformin suppressed HCV replication. HuH7.5.1 cells were infected with JFH1 and then treated with either metformin (A and B) or CsA (C and D) for 3 days. Densitometric values of NS5A normalized to those of β-actin were given as NS5A/β-actin. No significant cytotoxicity was observed by the compounds at the indicated concentrations. Relative HCV RNA level was quantified by real-time PCR and normalized to *GAPDH*; $^{*}p$ <0.05 or $^{\#}p$ <0.01 *vs.* untreated control. (E) In HuH7.5.1 cells either wild type or mutants (K81M or T208A) of FLAG-tagged SNARK were overexpressed and immunoprecipitated, followed by the detection with anti-FLAG or anti-phosphothreonine antibodies. (F) Wild type FLAG-tagged SNARK was overexpressed in the presence of metformin at 0.2, 0.5, and 1 mM in HuH7.5.1 cells and the levels of threonine phosphorylation were examined as indicated in (E). (G) HuH7.5.1 cells were transfected with either non-targeting (siNT-3) or *SNARK*-targeted (si*SNARK-8*) siRNAs. 48 hours later, cells were infected with JFH1 and treated with the indicated concentrations of metformin for 72 h. Relative mRNA levels for JFH1 or *SNARK* were quantified by real-time PCR and normalized to *GAPDH*.

[20], a well-known type 2 diabetes drug. In that setting, the kinase activity of SNARK was measured by incorporation of phosphate into SAMS peptide substrate, which was demonstrated to be significantly decreased by metformin treatment in the cell line. Here, we treated JFH1-infected HuH7.5.1 cells with metformin and observed moderate antiviral effects (Fig. 2A and B) with no cytotoxicity within the indicated dose range (data not shown). As a positive control, cyclosporin A (CsA) [21] strongly inhibited viral replication (Fig. 2C and D). To assess the phosphorylation level of SNARK subsequently, FLAG-tagged SNARK was overexpressed in HuH7.5.1 cells and immunoprecipitated for Western blot to monitor phosphothreonine levels [22]. While wild type SNARK was detected to be phosphorylated at threonine residue(s), neither K81M nor T208A mutant was (Fig. 2E), implying the autophosphorylation [23] and importance of threonine 208 as a phosphorylated site as reported [7]. Then we performed the assay using the wild type SNARK in the presence of metformin, which resulted in the reduced levels of phosphorylation dose-dependently (Fig. 2F). Here the data indicated that metformin suppressed SNARK phosphorylation, potentially interfering the phosphotransferase activity. The dose response of JFH1 to metformin was next examined when SNARK was knocked down by siRNAs. Metformin exerted dose-dependent antiviral effects in the cells transfected with non-targeting siRNAs, which was blunted by the siRNA-mediated reduction of SNARK expression (Fig. 2G). These data indicate that metformin's antiviral effect is mediated by inhibition of activated SNARK, bringing its full kinase activity, which may be a pharmacologic target for anti-HCV activity, and that metformin by itself could be a plausible component of a combination regimen targeting HCV.

SNARK is involved in TGF-β signaling

To investigate the possible roles of SNARK in viral pathogenesis based upon the induction of mRNA expression over the viral replication in cell culture (Supplementary Fig. 3), we also explored its involvement in downstream cellular signaling pathways. Intriguingly, SNARK appeared as an interactor with SMAD proteins in a high-throughput protein-protein interaction mapping study [17], which raised the distinct possibility that SNARK is involved in TGF-β signaling, the major profibrogenic pathway in the liver. Therefore, we first knocked down SNARK in HuH7.5.1 cells and assessed alterations in TGF-β signaling using an expression construct (PAI/L) encoding a luciferase reporter gene driven by promoter sequences of plasminogen activator inhibitor 1 (PAI-1), a transcriptional target of TGF-β [24]. siRNAs against *SNARK*